Source–sink turbulence in a rotating stratified fluid

By P. F. LINDEN, B. M. BOUBNOV† AND S. B. DALZIEL

Department of Applied Mathematics and Theoretical Physics, University of Cambridge,
Silver Street, Cambridge CB3 9EW, UK

In a recent paper Boubnov, Dalziel & Linden (1994) described the response of a stratified fluid to forcing produced by an array of sources and sinks. The sources and sinks were located in a horizontal plane and the flow from the sources was directed horizontally so that fluid was withdrawn from, and re-injected at, its own density level. As a result vertical vorticity was imparted to the fluid with a minimum of vertical mixing. It was found that when the stratification was strong enough to suppress vertical motions an inverse energy cascade was observed leading to the establishment of a large-scale circulation in the fluid. Those experiments were restricted to eight source–sink pairs. The present paper extends this work in two ways. First, up to forty source–sink pairs are used to force the flow, thereby producing a much wider separation of scales between the forcing and the flow domain. An inverse cascade is again found, but in this case the energy transfer to large scales is more rapid. The basic pattern of the large-scale flow is independent of the number of sources but the detailed structure depends on the energy input scale. Second, the effects of rotation about a vertical axis are investigated. It is found that when the Rossby deformation radius exceeds the size of the flow domain, the inverse energy cascade still occurs. However, for smaller values of the deformation scale, which in these experiments are comparable to or smaller than the forcing scale, the inverse cascade is altered by baroclinic instability. When flow structures develop on a scale larger than the deformation scale, usually by the merging of vortices of like sign, these structures are observed to split into smaller vortices of a scale comparable to the deformation scale. The flow appears to evolve with a balance between an anticascade produced by the two-dimensionality of the flow and a cascade due to baroclinic instability. For Rossby radii much smaller than the domain size the flow evolves into finite clumps of vorticity and an asymmetry between anticyclones and cyclones develops. A predominance of coherent anticyclones is observed, and the cyclonic vorticity is contained in more diffuse structures.

1. Introduction

Even the casual observer of the weather will have noticed that a major component of change is caused by the passage of high- and low-pressure systems. The Coriolis force associated with the Earth's rotation causes the air to flow around regions of high and low pressure which often form closed circulations. Similar circulating flows are observed in the oceans around pressure anomalies, and these 'mesoscale' eddies have received considerable attention in recent years. Oceanic mesoscale eddies have typical diameters of 100 km, while atmospheric weather systems have horizontal scales of the order of 1000 km. Recirculating flows are also found in planetary atmospheres with

† Permanent address: Institute of Atmospheric Physics, Moscow.

possibly the most striking example being Jupiter's 'Great Red Spot' with a horizontal scale of about 15000 km.

The horizontal scales of these motions are generally comparable to the relevant Rossby deformation radius associated with the ambient stratification and the local vertical component of the planetary rotation. Consequently, the dynamics of these flows are strongly influenced by both Coriolis and buoyancy forces. The vertical scale of these eddies is very much less than the horizontal scale and the motion within them is primarily horizontal. Vertical motions are also inhibited by the stratification and rotation, and typical values of the Froude number $Fr = U/Nh$, where U is a typical velocity, h is a typical vertical scale of the eddy and N is the buoyancy frequency, are in the range 0.01–0.1. The basic dynamics of these flows are quasi-geostrophic, with values of the Rossby number $Ro \leqslant 0.2$.

The two-dimensionalization of the flow, resulting either from stratification or the constraining effects of background rotation, leads, in general, to an inverse energy cascade. Energy is observed to accumulate in large scales and coherent structures emerge from a random initial background (McWilliams 1984; Legras, Santangelo & Benzi 1988 and Dritschel 1993). The accumulation of energy in these structures results from the inability of vortex lines to be stretched or twisted in a two-dimensional flow. Enstrophy (vorticity squared) does cascade to high wavenumbers and is dissipated by viscosity at small scales.

In a recent series of laboratory experiments, Boubnov, Dalziel & Linden (1994, hereafter referred to as BDL) have investigated the dynamics of the inverse energy cascade in stratified flows. Their experiments consisted of forcing a stably stratified region of fluid with an array of sources and sinks around the perimeter of a square tank. These sources and sinks induced horizontal motion in one horizontal plane, producing a turbulent flow. The flow was characterized by a forcing parameter $F_d = V/Nd$, where V is the velocity of the jets from the sources of diameter d, and N is the buoyancy frequency of the stratification. At high values of F_d three-dimensional turbulence was generated by the jets from the sources and this flow produced vertical mixing. Under these circumstances energy was observed to cascade to small scales as expected for three-dimensional flows. At low values of F_d the motion was primarily horizontal and an accumulation of energy in a large-scale circulation was observed. This energy transfer occurred once the vertical shear in the horizontal velocity had diminished due to viscous or wave-induced transfer of momentum away from the forcing layer, and an approximately two-dimensional flow was established.

The present paper is an extension of this work in two respects. The BDL the number of sources and sinks was restricted to eight pairs. In this paper we present results on the stratified case with up to forty source–sink pairs. As a consequence there is a much larger separation of scales between the forcing scale, as determined by the spacing between the sources and sinks around the boundary of the tank, and the scale of the domain. The second extension is to examine the effects of rotation on this flow. For this purpose the apparatus was mounted on a rotating turntable and spun with constant angular velocity about a vertical axis. We expect under these circumstances that the energy cascade to large scales will be affected by baroclinic instability at the Rossby deformation scale. Baroclinic instability provides a mechanism for the generation of smaller-scale motions which, at large amplitude, may lead to the formation of vortices. We observe the dynamics of these vortex structures and their influence on the energy transfer.

The format of this paper is as follows. In §2 the experimental apparatus is described, and the results for the non-rotating stratified flow are given in §3. The rotating

stratified case is discussed in §4 and some additional features of the flow, including the vertical structure of the flow and details of the vorticity field, are discussed in §§5 and 6. The conclusions of the work are discussed in §7.

2. The experiments

A sketch of the apparatus is shown in figure 1. The experiments were conducted in a rectangular Perspex tank of depth 445 mm, and with a square base measuring 610 mm. A circular ring of Perspex 10 mm thick, with inner diameter 563 mm, was suspended horizontally in the tank. In this ring eighty radial holes of 4 mm diameter were connected individually to eighty small pipes at the top of the ring. The holes had a right-angle bend, so that the orifices were in the inner vertical face of the ring. The eighty pipes were then connected in pairs through a peristaltic pump via small-bore tubing. Rearrangements of the tubing enabled up to forty source–sink pairs to be connected and experiments were carried out over the range eight to forty sources.

The construction of the ring ensured that the orifices were oriented along radial lines from the centre of the tank. In every case the active sources and sinks were arranged symmetrically around the circumference and equal flow rates provided from each of the sources. This arrangement ensured that the flow was forced symmetrically, and, within experimental error, no net impulse or angular momentum was imparted to the fluid. This arrangement of sources and sinks, therefore, removes fluid via the sinks at one horizontal level within the tank and re-injects it at the same horizontal level. The strength of the sources was controlled by the speed of the peristaltic pump, and this remained constant during any given experiment. We shall discuss in more detail the role of the sources and sinks in §7.

In order to study the effects of rotation the whole apparatus was mounted on a direct-drive, 1 m diameter, rotating turntable with a vertical axis of rotation. This turntable produces very accurate rotation rates with a consistency of better than 1×10^{-4} over a long period of time. The tank was filled with a linear salinity stratification produced by the standard 'double-bucket' method. When the tank was filled to the required depth the pump was run for a few minutes to clear any air from the tubing connecting the sources and sinks. Seeding particles were added for flow visualization and for particle tracking, and the system was left for a period to allow any residual motion to die away. In the rotating experiments the tank was filled while the turntable was rotating to facilitate the spin-up process and then left for several hours after filling to minimize any residual circulations in the flow.† When it was adjudged that the residual circulation was sufficiently weak, the experiment was started by turning on the pump and monitoring the flow over a period of time.

Flow visualization and measurements of the velocity field were obtained from video recording of the seeding particles placed in the flow. Pliolite VT particles approximately 0.5 mm in diameter were used as neutrally buoyant tracers for the flow. Pliolite VT is an opaque granular material used in the manufacture of paint. It may be ground and sieved to produce highly reflective particles of a desired size. By suitable choices of the density gradient the particles were located at the desired level within the flow and their motion was observed by a video camera mounted above the tank. For rotating experiments the camera was fixed to the turntable, so that the velocity measurements were obtained in the rotating frame. The particles were illuminated by a planar sheet

---

† It is impossible for a diffusive stratified fluid to remain in solid-body rotation as molecular diffusion drives a weak circulation (Griffiths & Linden 1985).
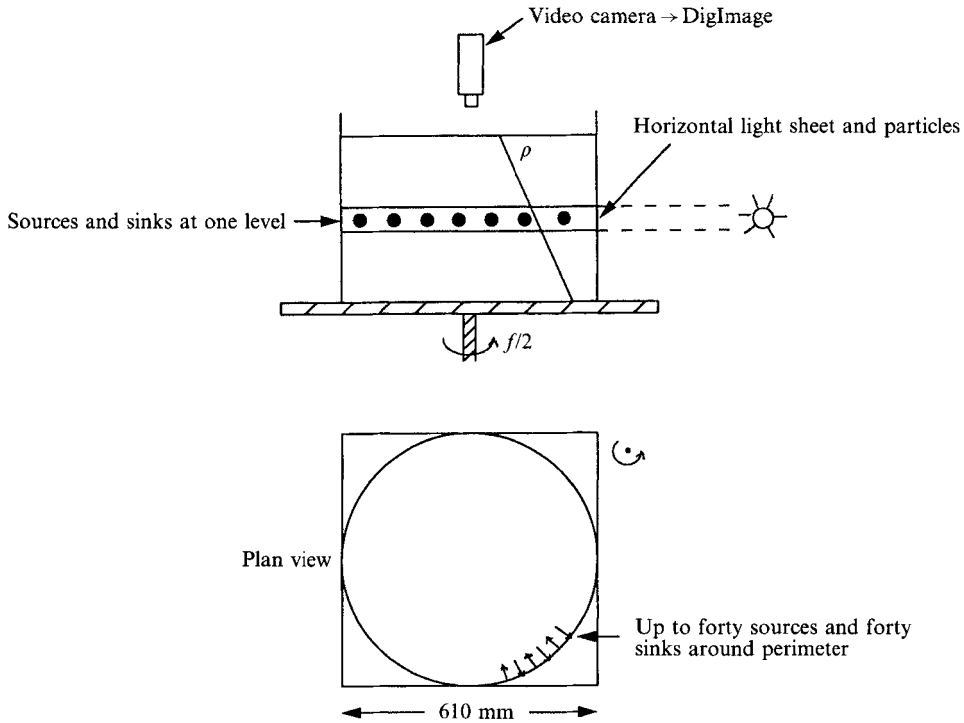
FIGURE 1. A diagram of the experimental apparatus showing the location of the sources and sinks and the arrangement for measuring particle motions in a horizontal plane. The video camera is fixed in the rotating frame.

of light from two slide projectors placed on opposite sides of the tank. In all the experiments a horizontal light sheet 5 mm thick was used and the flow velocities presented are the projections of the motion in this horizontal plane.

The video records of the flow were analysed using DigImage, a particle tracking system developed at DAMTP (Dalziel 1992, 1993), and described in detail in BDL. Typically, about 2000 particles were tracked in each frame and the velocities obtained by sampling the video film at a frequency of 6.25 Hz. Much of the information presented in this paper was obtained by mapping the velocity data onto a regular grid over the flow domain. The maximum error in the velocity grids is less than 5%, and the error in the derived vorticity field is better than 10%.

For a given fluid and geometric arrangement of sources and sinks there are five parameters governing the behaviour of the flow. These are the mean velocity V of fluid through the source orifices, the circumferential spacing between the sources l, the diameter of the orifices d, the buoyancy frequency $N = (g/\rho)(d\rho/dz)^{1/2}$, where $\rho(z)$ is the density, z is the height and g is the gravitational acceleration, and the Coriolis parameter is denoted by f. In the present experiments we have decided that the scale of the motion is better represented by l, the distance between the sources, rather than d the diameter of the orifices. These parameters may be expressed in terms of four non-dimensional external parameters: the forcing parameter $F = V/Nl$, the Reynolds number $Re = Vl/\nu$, where ν is the kinematic viscosity of the fluid, the ratio f/N of the Coriolis and buoyancy frequencies and the ratio l/d. The experiments considered here cover the range $0.046 < F < 4.2$, $540 < Re < 26000$, and $0 \leqslant f/N \leqslant 6.9$. The rotating unstratified ($N = 0$) case is also examined briefly. The forcing parameter F characterizes

Expt	n	N (s^{-1})	V (cm s^{-1})	f (s^{-1})	F	f/N	Re
12	8	1.0	2.0	0	0.085	0	4490
1102	20	1.0	3.5	0	0.26	0	2234
0601	40	1.0	2.2	0	0.48	0	1014
30	8	2.0	11.1	0	0.24	0	25600
19	8	1.0	11.1	0.4	0.47	0.38	25600
19a	8	1.0	11.1	1.6	0.47	1.57	25600
31	8	2.0	11.1	4.0	0.24	2.00	25600
24	8	1.0	11.1	4.0	0.47	3.85	25600
40	8	0.6	11.1	4.0	0.84	6.90	25600
23	8	0	11.1	2.0	∞	∞	25600
43	8	1.0	11.1	4.0	0.47	3.85	25600
41	8	0.6	11.1	3.2	0.84	5.52	25600

TABLE 1. Parameters for the experiments described in the text. The number of sources is represented by n, N is the buoyancy frequency, f is the Coriolis parameter. The Froude number F and the Reynolds number Re are defined in the text.

the relative strengths of the forcing and stratification. In BDL values of the forcing parameter and Reynolds number were defined in terms of the source diameter d by $F_d = V/Nd$ and $Re_d = Vd/\nu$, respectively, and are related to the values of F and Re here by $F = (l/d) F_d$ and $Re = (l/d) Re_d$, respectively. In BDL, $l = 100$ mm and $d = 4$ mm were fixed, so that $l/d = 25$. The Reynolds number gives a measure of the strength of the viscous forces, and Re_d is a measure of the Reynolds number of the flow from the orifices. The low values of Re_d in these experiments indicate that little or no fine-scale turbulence is injected into the flow.

At low F, the stratification inhibits vertical motion and it is expected that the flow will be predominantly horizontal. The ratio f/N gives the relative importance of the rotation and stratification effects on the flow. At large values of f/N we expect the motion to become more coherent in the direction parallel to the rotation axis. We shall relate F and Re to the internal properties of the flow in §6. Table 1 gives details of the experimental parameters.

3. Stratified non-rotating flow

The present experiments on non-rotating flows were designed to investigate the effects of changing the lengthscale of the forcing compared with that of the flow domain. They were restricted to low values of the forcing parameter F and, in the nomenclature developed in BDL, they lie in region II (large-scale circulation) on the regime diagram shown in figure 2 of that paper. In this regime, the flow is primarily two-dimensional and in the earlier experiments a large-scale circulation developed after a non-dimensional time $Nt \sim 10^4$. This corresponds to an elapsed time of about 4 hours for the values of N used in those experiments. The evolution of a similar flow in the present apparatus is shown in figure 2. This figure shows a sequence of velocity vectors determined from particle paths mapped onto a regular grid. The circle corresponds to the location of the ring containing the orifices of the sources and sinks, and the square corresponds to the boundary of the tank. Measurements were only taken over the flow domain within the ring but, of course, the fluid extends to the boundaries of the tank. In this case, and in all other flows presented in this paper except where it is stated explicitly, the particles are illuminated in a horizontal light sheet 5 mm thick, the top of which is located 1 mm below the bottom of the source–sink orifices. Hence the
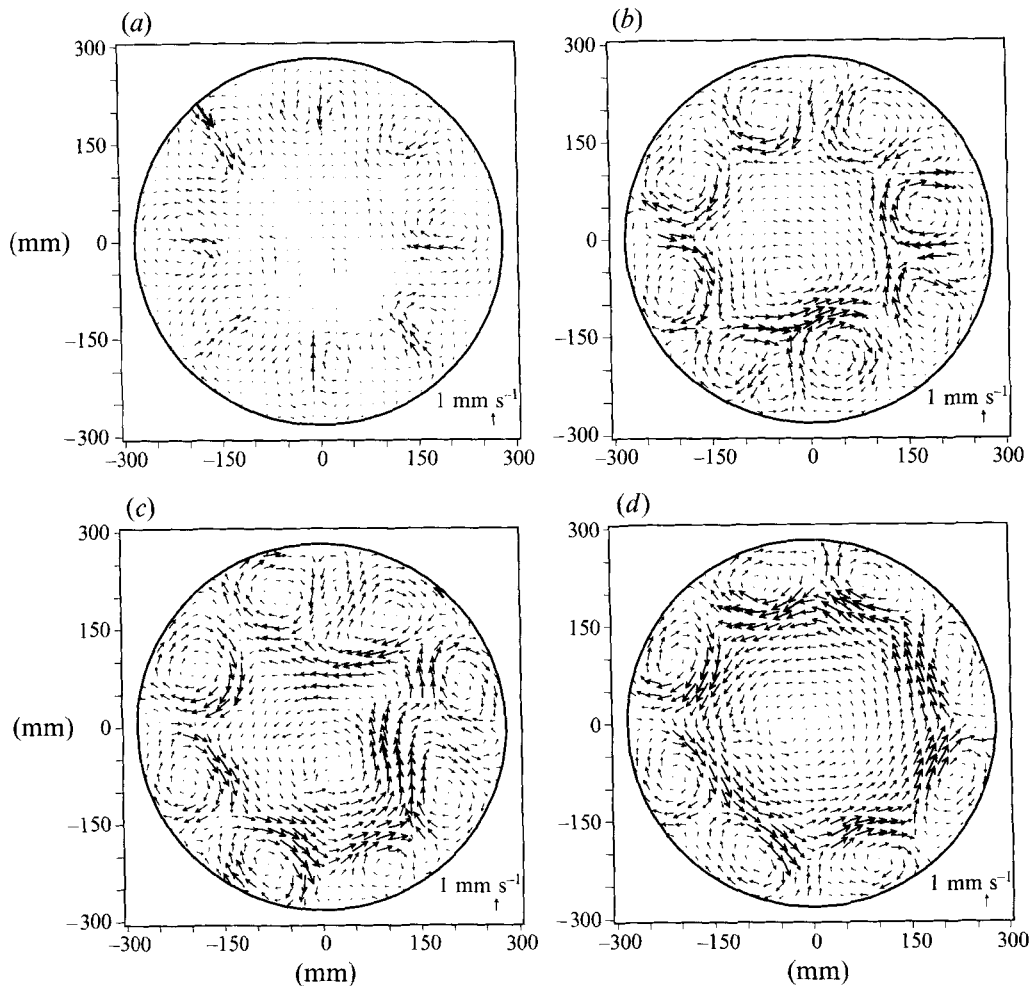
FIGURE 2. Velocity vectors for non-rotating stratified flow (Expt 12, $F = 0.085$, $Re = 4490$, $f/N = 0$) forced by eight source–sink pairs at four different stages in the development of the flow: (a) $Nt = 60$, (b) $Nt = 300$, (c) $Nt = 600$, (d) $Nt = 1200$. The flow is shown in a horizontal plane 5 mm thick the top of which is 1 mm below the bottom of the sources. The circle corresponds to the ring of the orifices of sources and sinks and the square corresponds to the boundary of the tank. The arrows in the bottom right corners show the velocity scale.

velocities are determined at a level as close as practicable to the level of the forcing. In BDL measurements were made in a plane 5 mm thick centred on the level of the sources. Hence there is a vertical overlap with the region examined here, and it confirms that the present results are an accurate measure of the flow at and near the forcing level.

The sequence of plots shows flow patterns from the earliest stages when the flow is being accelerated, through to the steady flow pattern which emerges after about 20 minutes ($Nt = 1200$). We see that as time progresses the flow from the sources penetrates towards the centre of the tank as is clearly shown in figure 2(c). The final state in figure 2(d) corresponds to a large-scale circulation in the interior of the domain with the influence of the eight circulations between the sources and sinks confined around the perimeter of the domain. Once this latter pattern is established it remains
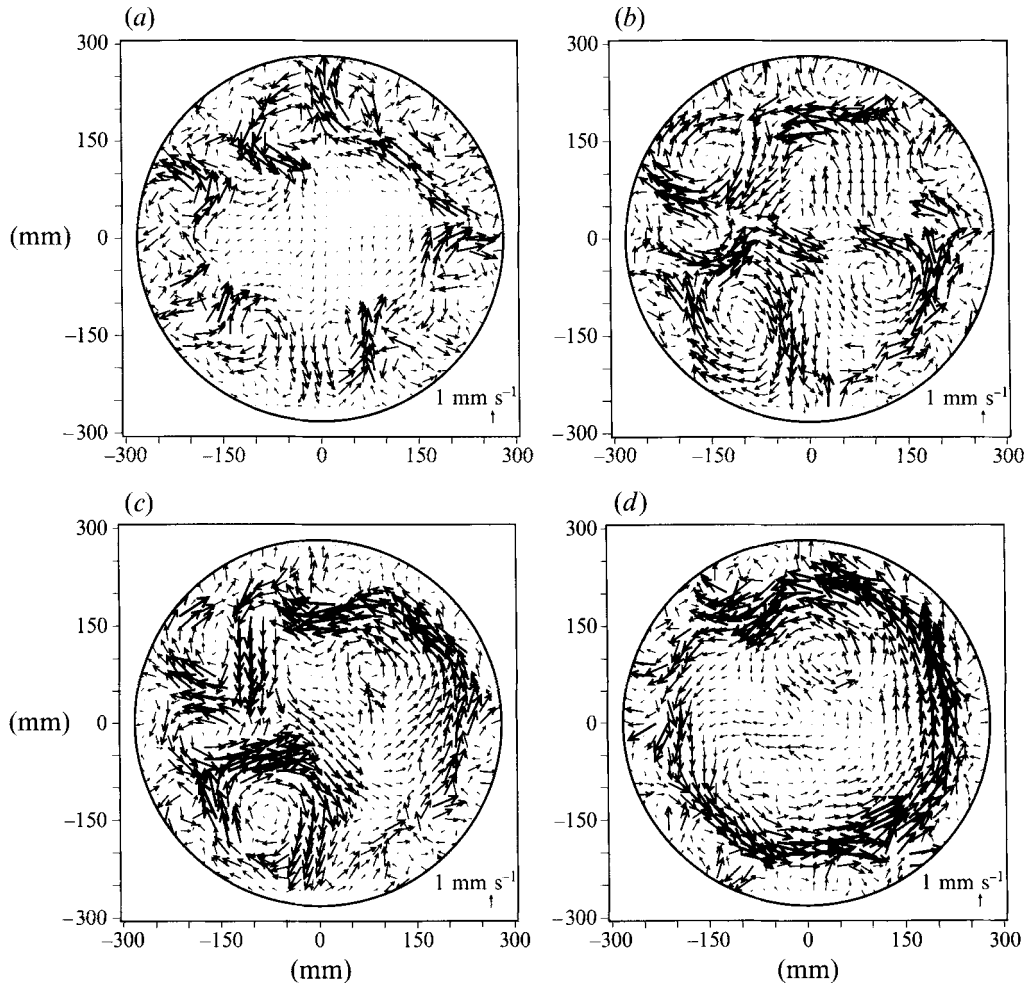
FIGURE 3. Velocity vectors for non-rotating stratified flow (Expt 1102, $F = 0.26$, $Re = 2234$, $f/N = 0$) forced by twenty source–sink pairs at four different stages in the development of the flow: (a) $Nt = 60$, (b) $Nt = 300$, (c) $Nt = 600$, (d) $Nt = 1500$.

unchanged, both in form and direction, for the duration of the experiment (up to several hours in some of the runs). In figure 2(d), we see that the circulation has its maximum speeds in a jet at the outer extremity of the eddies forced by the sources. The maximum velocities are comparable with the flow from the sources. Note that in the absence of vortex stretching it is not possible to generate velocities greater than the speed of the flow from the sources.

The flows shown in figure 2 correspond to those shown in figure 4 in BDL with the same number of sources at a similar spacing and the same values of F and Re; the only differences are the size of the domain and the orientation of the sources. In the present case, the sources are directed radially towards the centre of the domain, while in BDL they were perpendicular to the tank walls. There are a number of similarities in the observed flow patterns but also some important differences which result primarily from the larger flow domain in the present experiments. As was observed in BDL, there is a penetration of the motion into the interior of the tank (figure 2b) and the subsequent development of a large-scale circulation. For the present experiments the jets initially
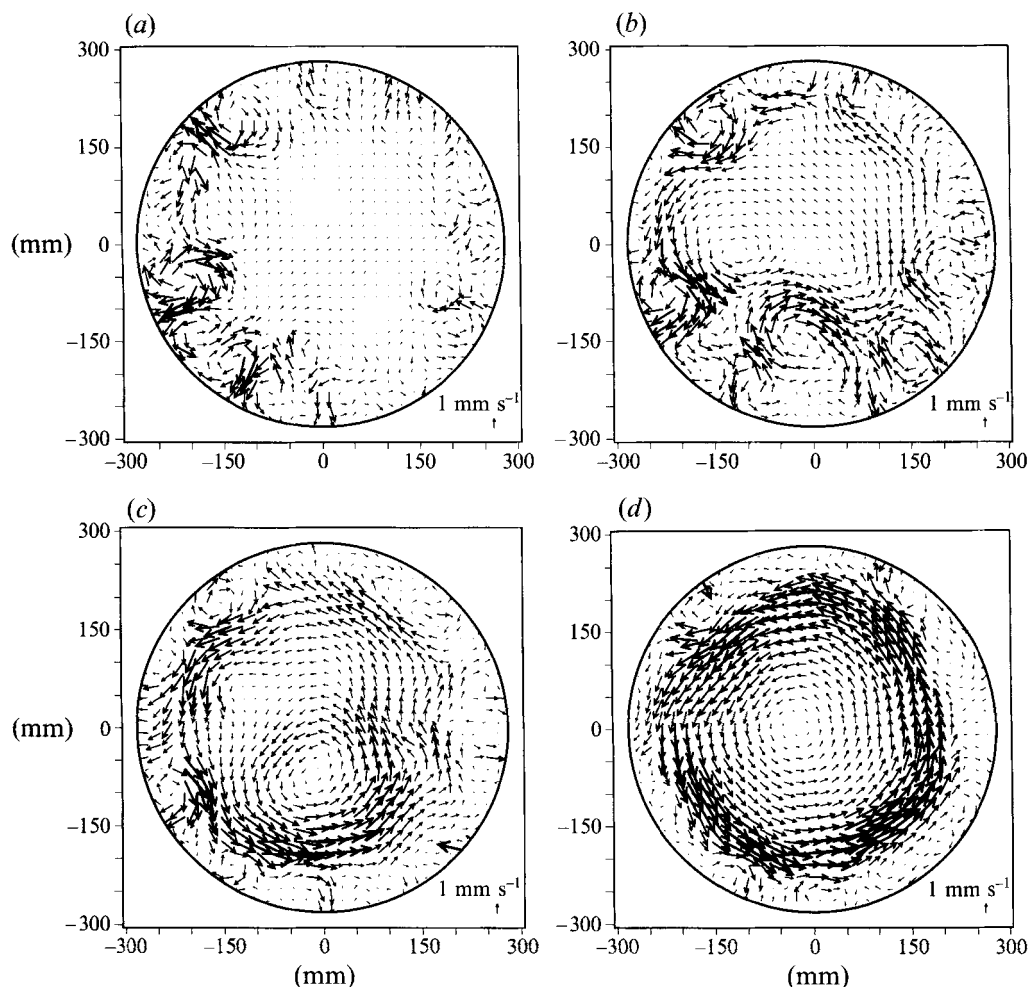
FIGURE 4. Velocity vectors for non-rotating stratified flow (Expt 0601, $F = 0.48$, $Re = 1014$, $f/N = 0$) forced by forty sources at four stages in the development of the flow: (a) $Nt = 60$, (b) $Nt = 300$, (c) $Nt = 600$, (d) $Nt = 1190$.

penetrate approximately 60 mm or 10% of the width of the domain and only a secondary motion propagates into the interior as can be seen from figures 2(b) and 2(c). In contrast, while the jets in BDL also penetrated approximately 60 mm, this was a much larger fraction of the domain, allowing vigorous motion to penetrate to the centre of the tank. Another difference is that in BDL the flow, at early times, exhibited significant vertical shear of the horizontal motion but there is little evidence of this shear in the present experiments. This reduction in the vertical shear seems to result from the spreading of the flow into the interior of the larger domain reducing the three-dimensional effects of the jets from the sources, and the flow appears to be more two-dimensional. The consequence of these differences is that the development of the large-scale circulation occurs much more quickly in the present experiments. In other respects, however, the flow has very similar qualitative characteristics to those observed in BDL.

The effects of reducing the forcing scale are shown in figures 3 and 4. Figure 3 shows the velocity fields for a flow forced with twenty sources and in figure 4 the flow is forced

with forty sources. In each case we see that the evolution of the flow patterns is very similar with the development of a large-scale circulation occurring after a time $Nt \sim 10^3$. The effect of decreasing the forcing scale can be seen in the scale of the motions around the perimeter of the large-scale circulations in these figures. In figure 2, eight clearly identifiable eddies are produced by the eight sources, while in figures 3 and 4 the scale decreases as the number of sources increases. The flow becomes much less organized around the boundary for this larger number of sources, and it is difficult to identify the flow from the individual sources in these cases. The flows depicted in these figures show that the development of the large-scale circulation is independent of the scale of the forcing and that it arises spontaneously as a result of energy transfer from small scales to large scales. Observations of these flows using video recordings shows that the increase in scales occurs by merging of vortices of like sign. Interactions of vortices of opposite sign produce a smearing out and destruction of the weaker vortex and, hence, a single dominant circulation is produced.

The time evolution of the large-scale circulation has some different features as the number of sources is increased. For the eight-source case shown in figure 2 there is little evidence of small-scale features propagating in towards the centre of the flow domain. The large-scale circulation develops around the edges of the vortices directly forced by the sources and the initial penetration of the motion into the interior of the tank is relatively weak. In contrast, the flows shown in figures 3 and 4 show an increased penetration of the motion into the interior in the early stages. This motion is then expelled from the centre of the tank, and the velocity shear and, therefore, the vorticity accumulates in the outer edge of the large-scale circulation. This effect is shown particularly clearly in figures 3(d) and 4(d). In all cases the magnitude of the velocity in the large-scale circulation is comparable with that from the sources.

Another feature to note is that while the forcing parameter F_d and the Reynolds number Re_d *for each source individually* are approximately the same in figures 2–4, the kinetic energy imparted to the flow increases in proportion to the number of sources. Therefore, the energy input to the flow shown in figure 4 is five times that shown in figure 2. This increase in energy may account for the increased penetration of the flow into the interior of the domain in the latter case. The increased penetration of vortices into the interior of the tank results from the cooperative interaction between these vortices. An example of inward motion produced by a pair of vortices of opposite sign can be seen at 8 o'clock in figure 3(b). It is also evident from a comparison of figures 2(d), 3(d) and 4(d) that the energy of the large-scale circulation increases with the number of sources, which seems to be consistent with the energy imposed by the forcing. Measurements of the mean velocities averaged along x and y lines over the flow domain show that the net circulation $\int \boldsymbol{u} \cdot \mathrm{d}\boldsymbol{r}$ is extremely small, a result which is consistent with the fact that the forcing is symmetric. The circulation associated with the large-scale flow is, therefore, cancelled by the structures around the edge providing a negative vorticity which gives, as required, a zero circulation taken around the outer boundary of the flow. It should be emphasized that this flow domain is not the physical exterior of the tank as velocities have only been tracked over the central ring containing the sources and sinks.

It will be noted in figures 2–4 that the direction of the large-scale circulation is anticlockwise in each case. This direction was a consistent feature of all these experiments, and appears to be related to some weak bias in the forcing mechanism. It seems that the sense of this large-scale circulation is set by irregularities in the forcing which are too small to detect by other means. In the earlier experiments reported in BDL the sense of the circulation was observed to be in both clockwise and

anticlockwise directions and this variation in flow direction was presumably as a result of small changes in the position of the (moveable) sources and sinks between experiments. The new arrangement for the sources and sinks in the present experiments means that the bias is set according to the accuracy of machining the orifices in the circular ring. Consistent with our earlier observations, the circulation once developed remained in the same direction for as long as the experiment was continued.

As a result of these observations we conclude that the increase in the number of sources produces mainly quantitative changes to the development of the flow. Despite some differences in detail the basic qualitative features observed in BDL are reproduced here with a wider separation between the forcing and the domain scales. We turn now to the effects of rotation on these flows.

4. Stratified rotating flow

As was mentioned in §2, when the apparatus is rotated about a vertical axis a weak diffusion-driven circulation is generated within the tank. This circulation is a result of diffusion across isopycnals which are parabolic in the interior of the tank but horizontal at the tank walls. This departure of the isopycnals from the geopotentials leads to flow up the sides of the tank which is returned to the interior in such a way as to compress vortex lines and drive a weak anticyclonic flow. In the present experiments we observed diffusion-driven circulations of about $5 \mathrm{~mm} \mathrm{~s}^{-1}$ and, as a result, it was not possible to investigate very low source flow rates, since the strength of the flow was then only comparable with this diffusion-driven circulation. Therefore, the results that we present below for the rotating case concentrate on values of the forcing parameter F where the velocities are significantly greater than this circulation. In order to achieve these larger flow rates and to work within the capacity of the peristaltic pump, it was necessary to restrict the number of sources to eight. In the light of the results presented in §3 we believe this restriction does not represent a serious limitation on the generality of these observations. It does, however, mean that only a single forcing scale is examined in these rotating flows.

The effects of increasing rotation are illustrated in figures 5–11, which cover a range of values of f/N from zero (non-rotating flows), to infinity (unstratified flows). As for the non-rotating flows described in §3, the forcing parameter F_a for each individual orifice is the same in these experiments. The non-rotating case illustrated in figure 5 for $F = 0.24$ shows again the development of a large-scale circulation as discussed in §3. At this higher value of the forcing parameter the effects of the individual sources are more significant, and we see that the large-scale circulation is confined more to the centre of the tank than the eight-source flow at lower F shown in figure 2. Nevertheless, the particle paths from which the data shown in figure 5 are calculated are correlated over the vertical extent (5 mm) of the light sheet and indicate that the motion is broadly two-dimensional. As a result this flow appears to lie in regime II described in BDL, although the value of the forcing parameter is at the upper extreme of the regime determined in that series of experiments. A comparison of figure 5 with figure 3 illustrates the effects of changing the forcing scale at a constant value of F. The maximum velocities observed within the flow are comparable (note the change in the scale of the velocity vectors) despite the fact that the efflux velocities from the sources in Expt 30 (figure 5) are more than three times larger than those in Expt 1102 (figure 3). However, the increase in the forcing scale in the latter experiment causes the large-scale circulation to be broader and to be pushed further into the centre of the tank, and so the flows are not concentrated into such thin streams.
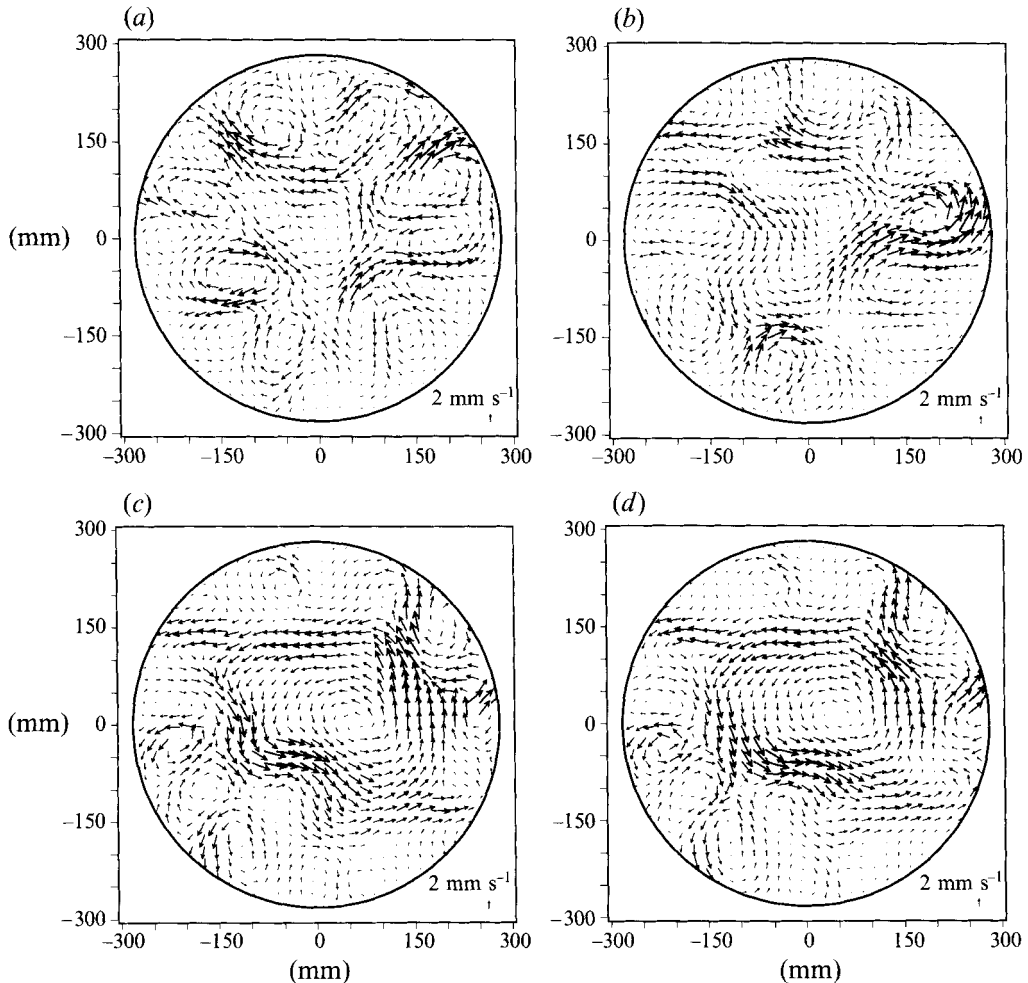
FIGURE 5. Velocity vectors for non-rotating stratified flow (Expt 30, $F = 0.24$, $Re = 25600$, $f/N = 0$) forced by eight sources at four stages in the development of the flow: (a) $Nt = 120$, (b) $Nt = 600$, (c) $Nt = 1200$, (d) $Nt = 1800$.

The effects of rotation, as described by increasing values of f/N at similar values of F and Re and with the same number of sources, are shown in the successive figures 6–11. Figure 6 shows the flow in the case $f/N = 0.38$, $F = 0.47$. In this case the flow develops a large-scale circulation surrounded by smaller-scale eddies on the scale of the forcing at the outer part of the flow domain. The direction of the background rotation is positive, and the large-scale circulation shown in figures 6(c) and 6(d) is cyclonic and the two eddies which appear to be the dominant smaller-scale features in figure 6(d) are anticyclones. This sense of circulation of the large-scale flow is the same as that found as a consistent feature in the non-rotating cases, and is again probably due to some bias in the forcing arrangement. In the rotating case, however, it is consistent with inflow from the sources towards the centre of the tank producing convergence, and it is in the opposite sense to the diffusion-driven circulation which is anticyclonic. Consequently, we are unable to determine whether the sense of this circulation is influenced by rotation, but the fact that it opposes and overcomes the bias associated with the diffusion-driven circulation that is present before the pumping starts suggests
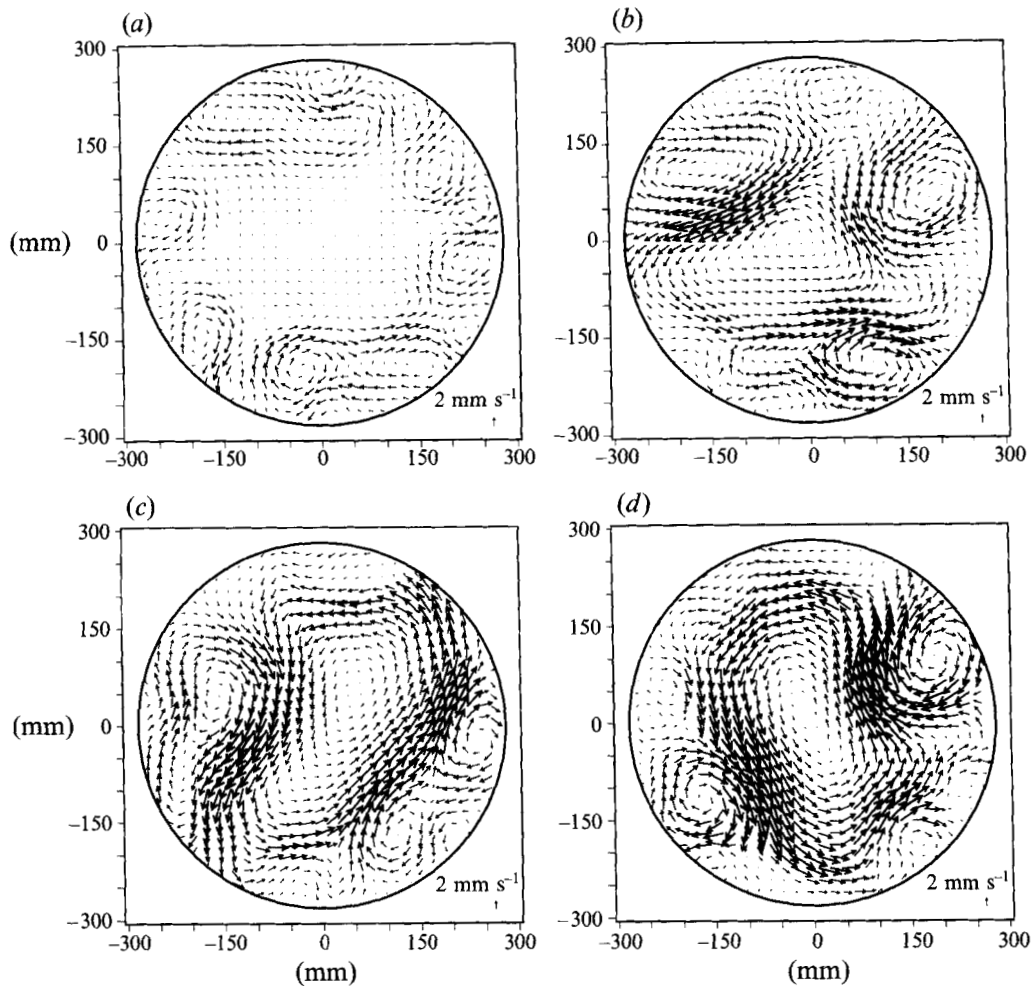
FIGURE 6. Velocity vectors for rotating stratified flow (Expt 19, $F = 0.47$, $Re = 25600$, $f/N = 0.38$) at four stages in the development of the flow: (a) $Nt = 60$, (b) $Nt = 300$, (c) $Nt = 600$, (d) $Nt = 1200$.

that it probably is. The Rossby deformation scale corresponding to the lowest baroclinic mode is $R_D = NH/f$ is 750 mm, based on the full depth H of the tank. This scale is larger than the flow domain and so we expect the effects of rotation to be weak. The similarities between the flows shown in figures 5 and 6 support this conjecture, in that the large-scale flow develops on a very similar timescale. Structures with smaller vertical scales are affected by rotation on smaller horizontal scales, and the details of the barotropization process are not entirely clear. Some further discussion of this point is given in §7. In the rotating case the large-scale circulation is faster, with velocities about twice that of the non-rotating flow. The circulation is also less circular and extends closer to the sources and sinks. In addition, the pattern is less stable and varies considerably with time, with the vortices produced by the sources propagating around the outside of the circulation.

Figure 7 shows the effects of increasing the rotation rate and gives examples of the flow evolution for the case $f/N = 1.57$, $F = 0.47$. In this case we see a marked change in the evolution of the flow. In particular, the large-scale circulation does not develop.
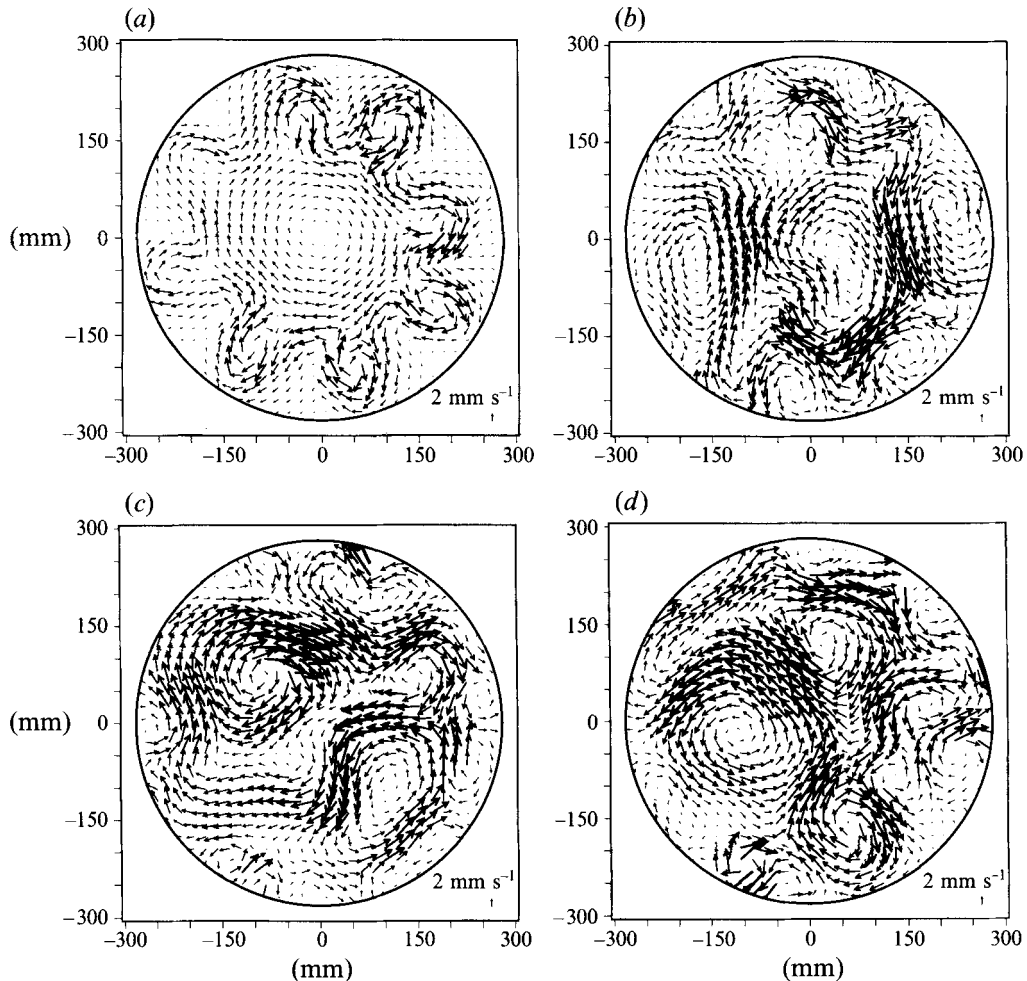
FIGURE 7. Velocity vectors for rotating stratified flow (Expt 19a, $F = 0.47$, $Re = 25600$, $f/N = 1.57$) at four stages in the development of the flow: (a) $Nt = 60$, (b) $Nt = 300$, (c) $Nt = 540$, (d) $Nt = 1200$.

The early stages of the flow after the forcing is started, shown in figures 7(a) and 7(b), suggest that the flow initially evolves with a large-scale circulation developing (note the anticyclonic diffusion-driven circulation present at the earliest time shown in figure 7a). An initial series of eight vortices are formed linked to the eight source flows. In this case, these vortices are all anticyclones which suggests that the outflow from a source is affected by the Coriolis force. These vortices then move into the interior of the flow (figure 7b), and there is evidence of a large-scale cyclonic circulation developing. However, this large-scale circulation does not evolve as in the cases of lower and zero rotation rate but, instead, appears to break up into a series of smaller-scale eddies. This evolution can be clearly seen in figures 7(c) and 7(d). In the ultimate state of the flow there is motion on two scales. The sources continue to produce relatively small-scale structures around the boundary of the domain while eddies of larger scale, but significantly smaller than the domain size, are found in the interior. The scale of the eddies in the interior of the domain is approximately equal to the Rossby deformation scale, $R_D = 180$ mm. Both cyclones and anticyclones are observed. At the latest stage
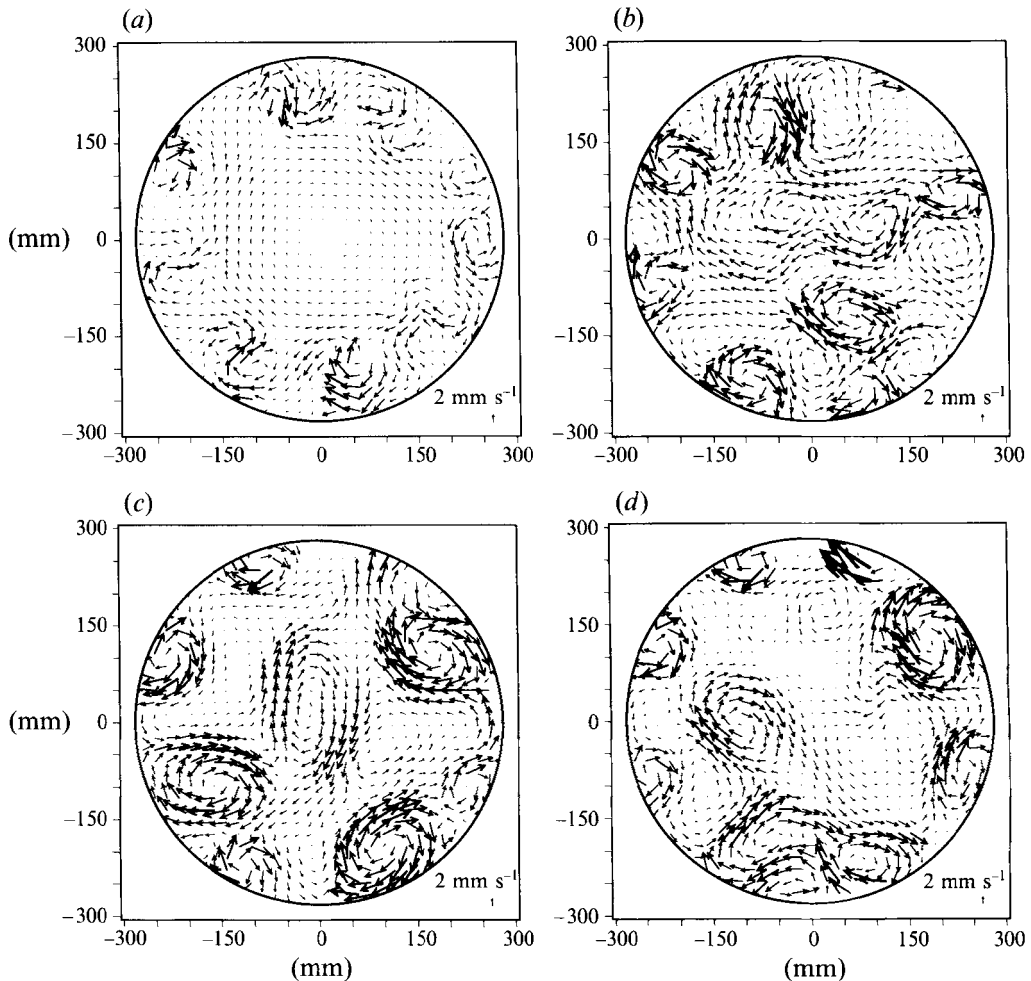
FIGURE 8. Velocity vectors for rotating stratified flow (Expt 31, $F = 0.24$, $Re = 25600$, $f/N = 2.00$) at four stages in the development of the flow: (a) $Nt = 120$, $Nt = 600$, (c) $Nt = 1200$, (d) $Nt = 1800$.

of the flow shown in figure 7(d), there are four cyclones and six anticyclones which fill the flow domain. The Rossby numbers of the vortices $Ro = |\omega/f|$, where ω is the vertical component of the relative vorticity, are fairly small with $Ro \leqslant 0.4$.

Further increases in rotation rate enhance these trends. Figure 8 illustrates the flow for $f/N = 2.0$, $F = 0.24$ and figure 9 shows the evolution for the case $f/N = 3.85$, $F = 0.47$. Here again we see the breakdown of the large-scale diffusion-driven circulation present at early times into a series of small-scale eddies. In these examples the eddies in the interior of the flow are comparable in size with those around the boundary of the domain and they occupy all parts of the flow domain. At these higher values of f/N the vortices appear to become isolated and are separated by regions of relatively quiescent flow. The scales of the vortices are again consistent with the deformation scale R_D. The sign of the eddies is now predominantly anticyclonic in contrast to the example shown in figure 7. Similar features are shown in figure 10 for the case $f/N = 6.9$, $F = 0.84$. Here again the predominance of anticyclones in the final stages is observed, and the eddies are now clearly separated in space and vorticity is confined into finite clumps. The Rossby number for these vortices is $Ro \leqslant 0.3$.
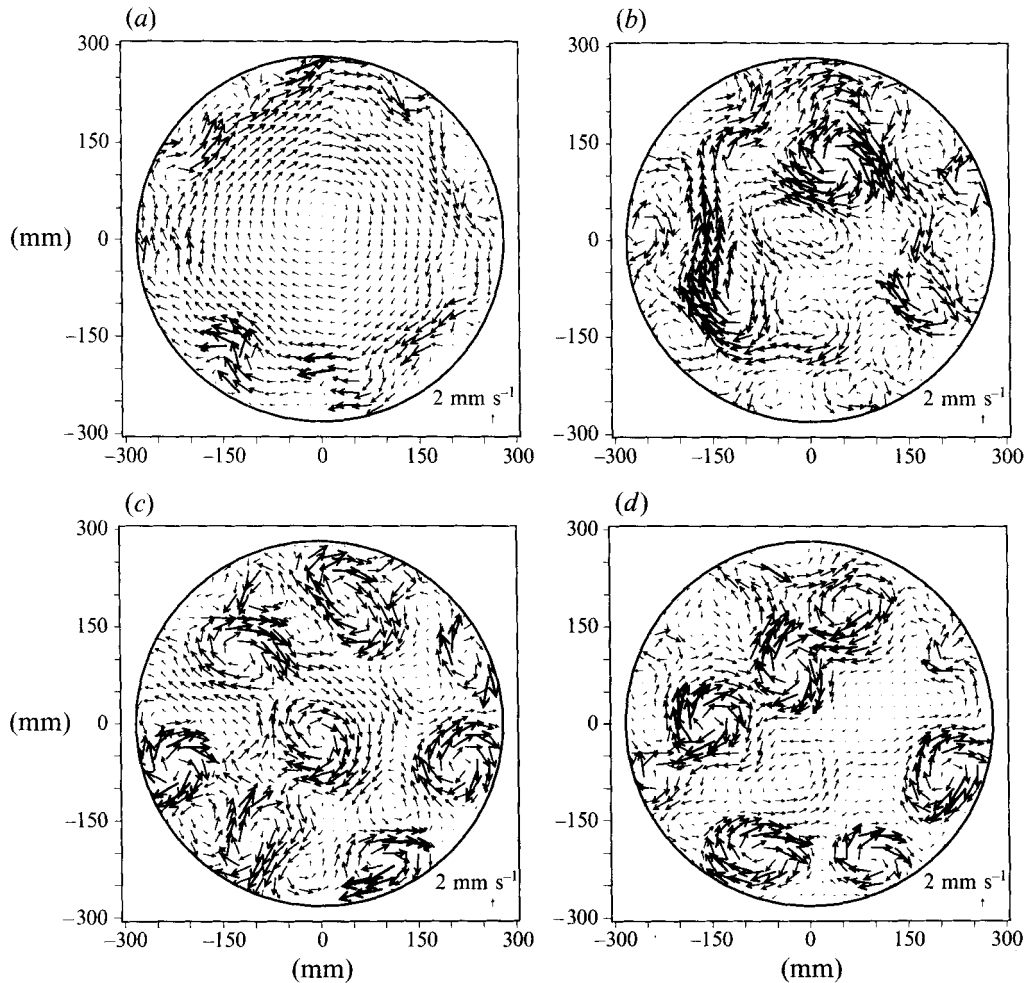
FIGURE 9. Velocity vectors for rotating stratified flow (Expt 24, $F = 0.47$, $Re = 25600$, $f/N = 3.85$) at four stages in the development of the flow: (*a*) $Nt = 60$, (*b*) $Nt = 300$, (*c*) $Nt = 600$, (*d*) $Nt = 900$.

The final example is shown in figure 11 which shows a case of an unstratified fluid in the presence of background rotation. Here the motion is concentrated in the region adjoining the sources and the figure shows the vertical coherence of the flow by tracking particles both at the level of the sources and at the surface. Each vortex is an anticyclone as a result of the Coriolis force pushing the jet from the source to the right. As has been found in other experiments (Colin de Verdiere 1980) the vortices in this case interact only through Ekman layers and the development of the flow is completely different from the stratified situation. As a result the flow is confined to vortices adjacent to the sources, and the lack of vortex interactions means that upscale energy transfers do not occur. Although, as figure 11 shows, the motion is two-dimensional, the absence of nonlinear interactions caused by the strong coupling of the vortices to the bottom Ekman layer makes the unstratified case anomalous. For this reason we do not consider it further.

In summary, therefore, the effects of increasing rotation are to reduce the scale of the eddies that are produced and to lead to predominance of anticyclonic motion. This
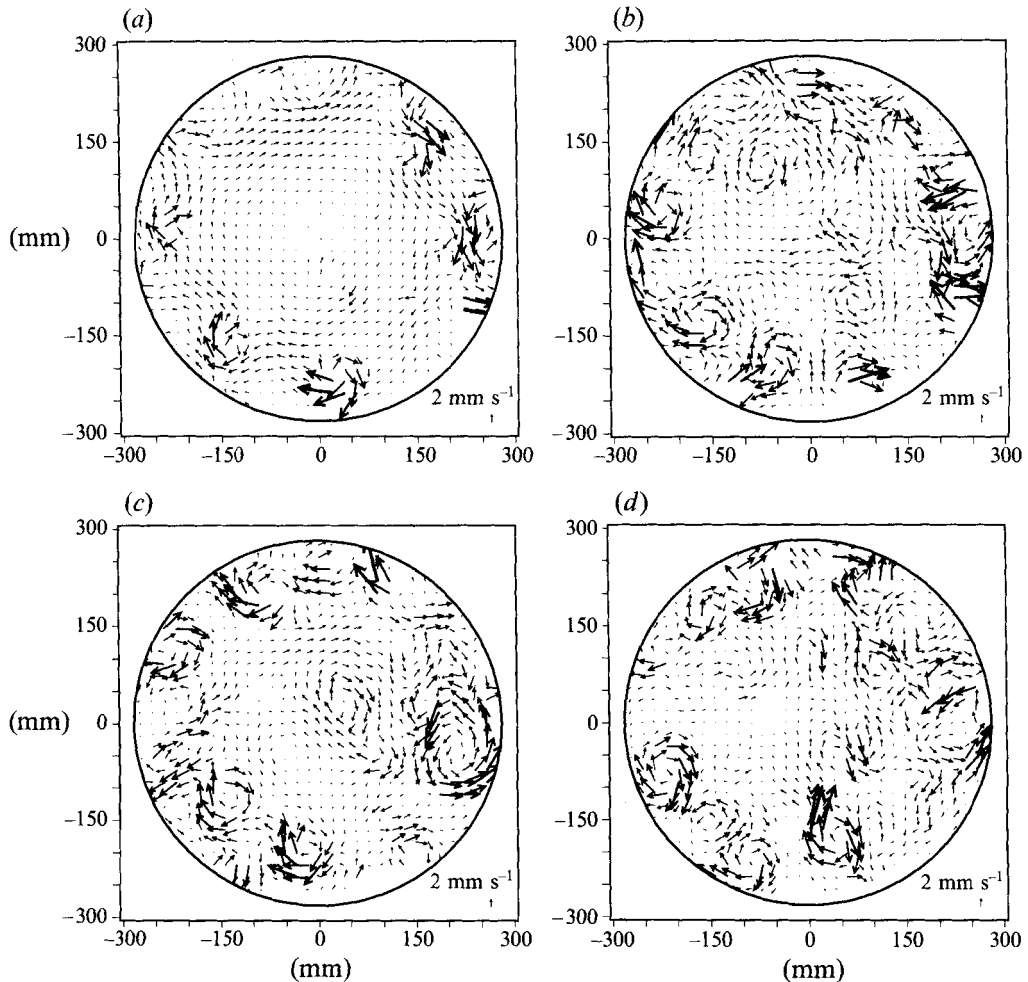
FIGURE 10. Velocity vectors for rotating stratified flow (Expt 40, $F = 0.84$, $Re = 25600$, $f/N = 6.90$) at four stages in the development of the flow: (a) $Nt = 35$, (b) $Nt = 174$, (c) $Nt = 348$, (d) $Nt = 522$.

reduction in scale is consistent with the reduced Rossby deformation radius at large rotation rates, and would suggest that the flow is unstable to baroclinic instability. Sloping isopycnal surfaces result from the induced large-scale flows which break up when their scale exceeds the deformation radius (Griffiths & Linden 1981; Holford 1994). The release of potential energy from the stratification by this baroclinic instability leads to the production of smaller scales at high rotation rates and confines most of the vorticity to coherent vortex structures.

Figure 12 shows the velocity vectors from the final state of four experiments with increasing values of f/N. In this figure the vertical component of the relative vorticity ω is calculated from the observed velocity field and the contours are shown in the false colour images. In the non-rotating case (figure 12a) the values of $|\omega|$ are relatively small, but $|\omega|$ increases with increasing f. As described above, strong anticyclones emerge in the rapidly rotating cases, and the scale of the vortices decreases with increasing rotation rates. The Rossby numbers Ro of the vortices decrease with increasing rotation (see also figure 18) implying that the flows become more geostrophic as rotational effects become more important.
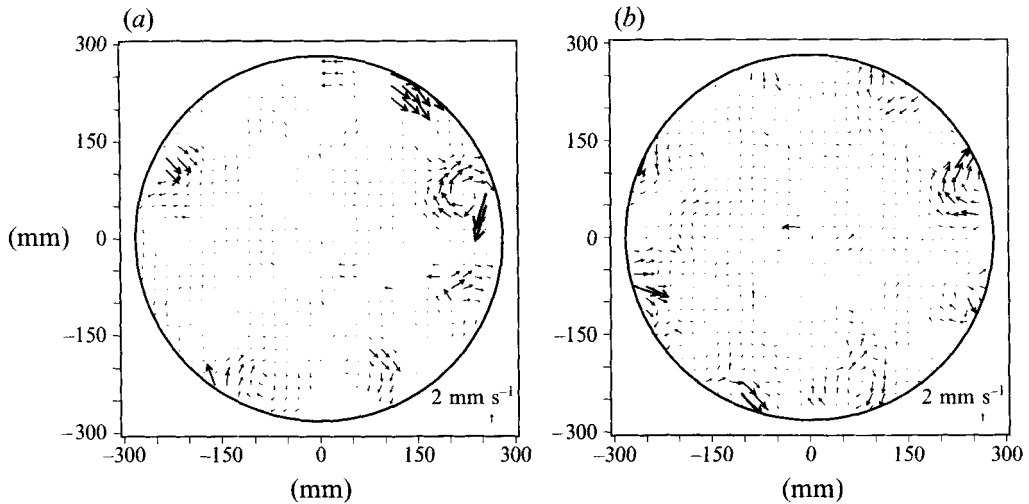
FIGURE 11. Velocity vectors for rotating unstratified flow (Expt 23, $Re = 25300$) at the forcing level (*a*) and at the surface (*b*). Note how the vortices are trapped next to the sources. Each vortex is an anticyclone as a result of the Coriolis force acting on the jet from the source.

Further information on the time evolution of these flows is given in figure 13, which shows the r.m.s. fluctuating velocities plotted against time for four different values of f/N. The velocity components u (solid line) and v (broken line) are referred to x and y Cartesian axes aligned across and up the page for the plots shown in the figures 2–11. In the non-rotating case, figure 13(*a*), there is little difference between the two components. The flow accelerates quickly over the first 100 s: this flow has forty sources and the flow patterns are shown at 60 s and 300 s in figures 4(*a*) and 4(*b*), respectively. During this initial phase the flow from the sources penetrates into the interior. The flow continues to accelerate at later times but at a much reduced rate. There is evidence that the velocities are still increasing at the end of the measurements, suggesting that the flow has not reached a steady state.

The continued increase in the r.m.s. velocities in figure 13(*a*) suggests that the flow is continuing to diffuse vorticity vertically into the regions above and below the forcing level. The large-scale circulation is established at about 600 s, and the qualitative nature of the flow then remains unchanged. The effect of increasing rotation rates is shown in figures 13(*b*) $f/N = 0.19$, 13(*c*) $f/N = 0.8$ and 13(*d*) $f/N = 3.85$. In these rotating cases the acceleration phase is extended with the flow, taking approximately 200 s to be established in each case. For the lowest rotation rate $f/N = 0.19$ this corresponds to three rotation periods while for the fastest rotating rate $f/N = 3.85$ the flow accelerates over approximately seventy rotation periods. Once this initial acceleration phase is over, the flow appears to be in an approximate steady state with velocities in the rotating cases being considerably larger than those in the non-rotating case. This increase in velocity results from the fact that rotating cases are for eight source flows compared with the forty sources in the non-rotating case, figure 13(*a*). It is also noted that there are low-frequency oscillations in the velocity signals with the u- and v-components being out of phase. The cause of these fluctuations is unknown but they may be produced by wave modes within the tank. There is a general increase in frequency of these fluctuations with increasing rotation rate, which results from the increased variability associated with the smaller-scale eddies at the higher rotation rates. The rapid fluctuations in the non-rotating case, figure 13(*a*), result from the
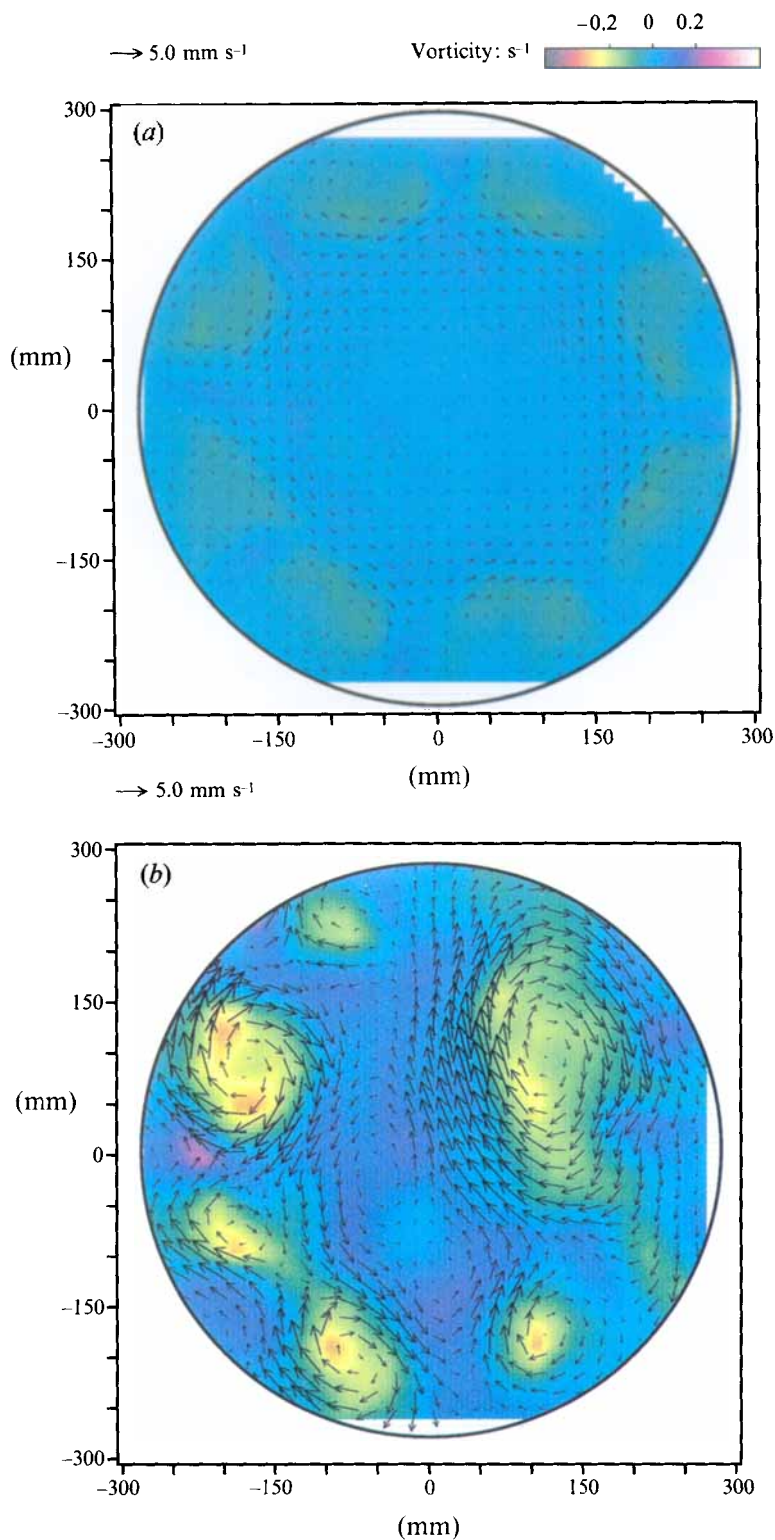
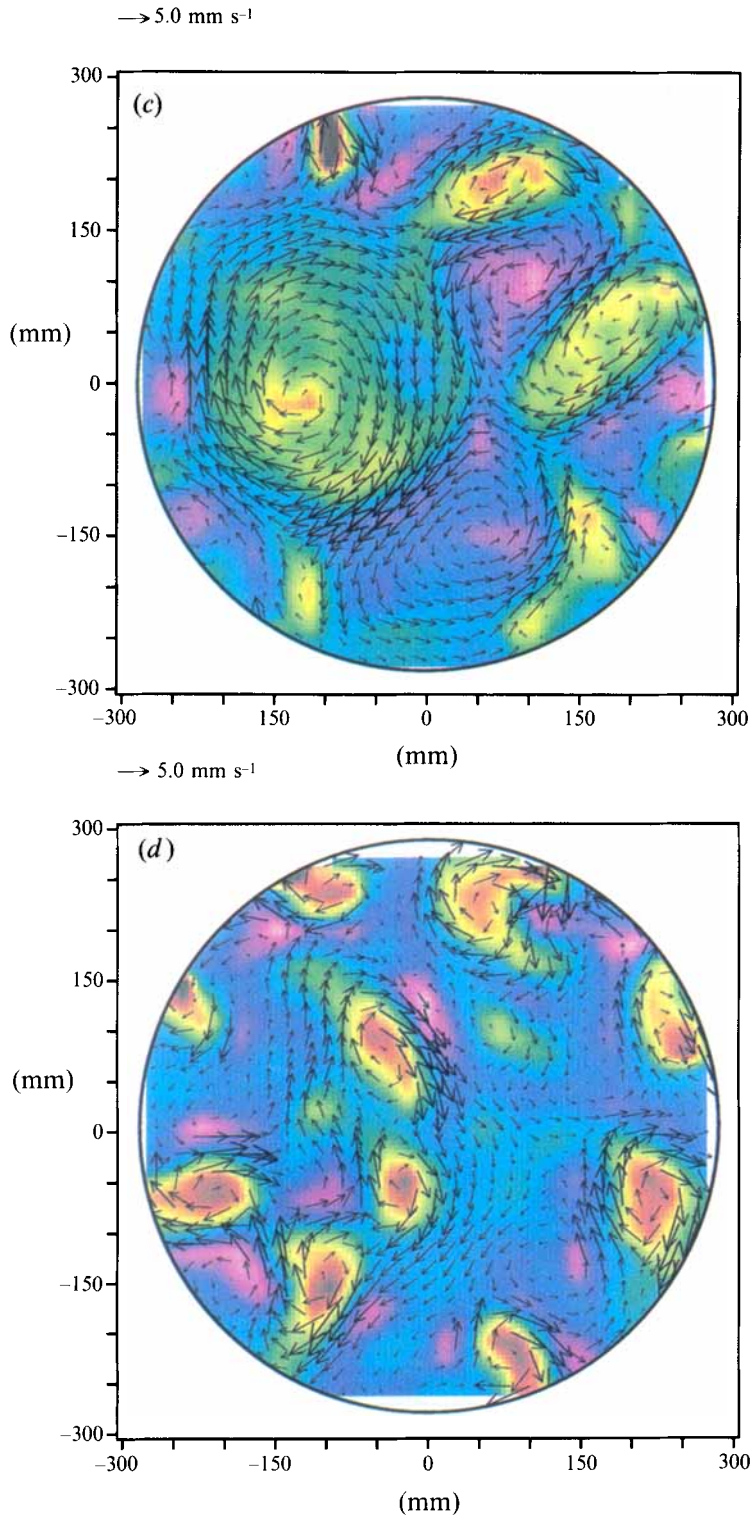FIGURE 12 (*a*, *b*). For caption see facing page.

FIGURE 12. Velocity vectors and vorticity contours for eight-source flows for (*a*) $f/N = 0$, (*b*) $f/N = 0.8$, (*c*) $f/N = 1.6$ and (*d*) $f/N = 4.0$. The flows shown are representative of the ultimate states of these systems.
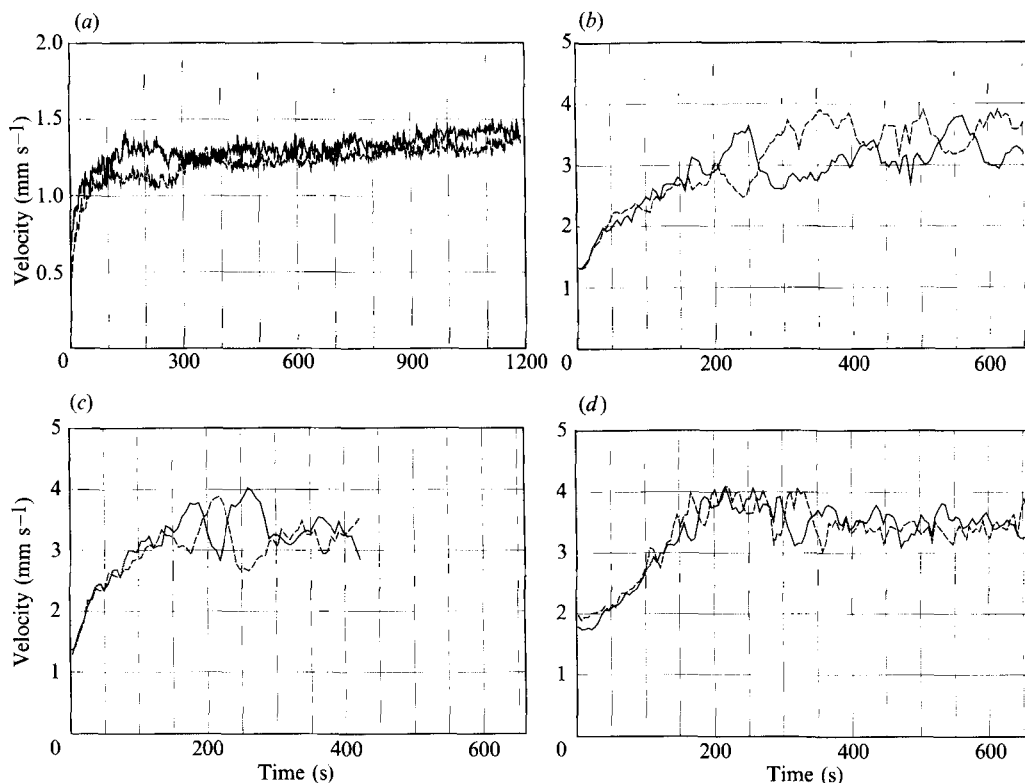
FIGURE 13. Root-mean-square fluctuating horizontal velocities plotted against time for (a) $f/N = 0$, (b) $f/N = 0.38$, (c) $f/N = 0.8$ and (d) $f/N = 3.85$. The velocity is resolved into two components u (——) and v (– – –) relative to x- and y-axes aligned with the horizontal and vertical sides of the flows in figures 2–11.

variability associated with the smaller lengthscale of the forcing in that case compared with those in figure 13(b–d).

All the eight-source experiments shown in figure 12 are at a fixed Reynolds number $Re = 25600$. In the non-rotating case BDL found little dependence on Re and argued that viscous effects are not important in the vortex interactions and the transport of vorticity into the interior of the domain. The dissipation mechanism for the large-scale circulation is not clear: it may be due to viscosity, internal wave radiation or some combination of the two. In either case, the dissipation mechanisms are weak and the large-scale flow has a long decay time. In the rotating case the question of dissipation is more complex as Ekman layers form on solid boundaries. Since the fluid is stratified, the effects of Ekman pumping are much reduced compared with the unstratified case. Thus we believe that dissipation will again occur either directly by viscosity or by radiation of inertial-internal gravity waves. This aspect of the flow has not been addressed in detail, but some related issues concerning the vertical structure of the flow are discussed in the next section.

5. Vertical extent of the vortex motion

The vertical coherence of the flow is a function of the strength of the rotation. The stratification damps the vertical velocities w, while rotation reduces the vertical shear in the horizontal velocity $\partial u/\partial z$ and $\partial v/\partial z$. As the rotation increases, we expect the flow
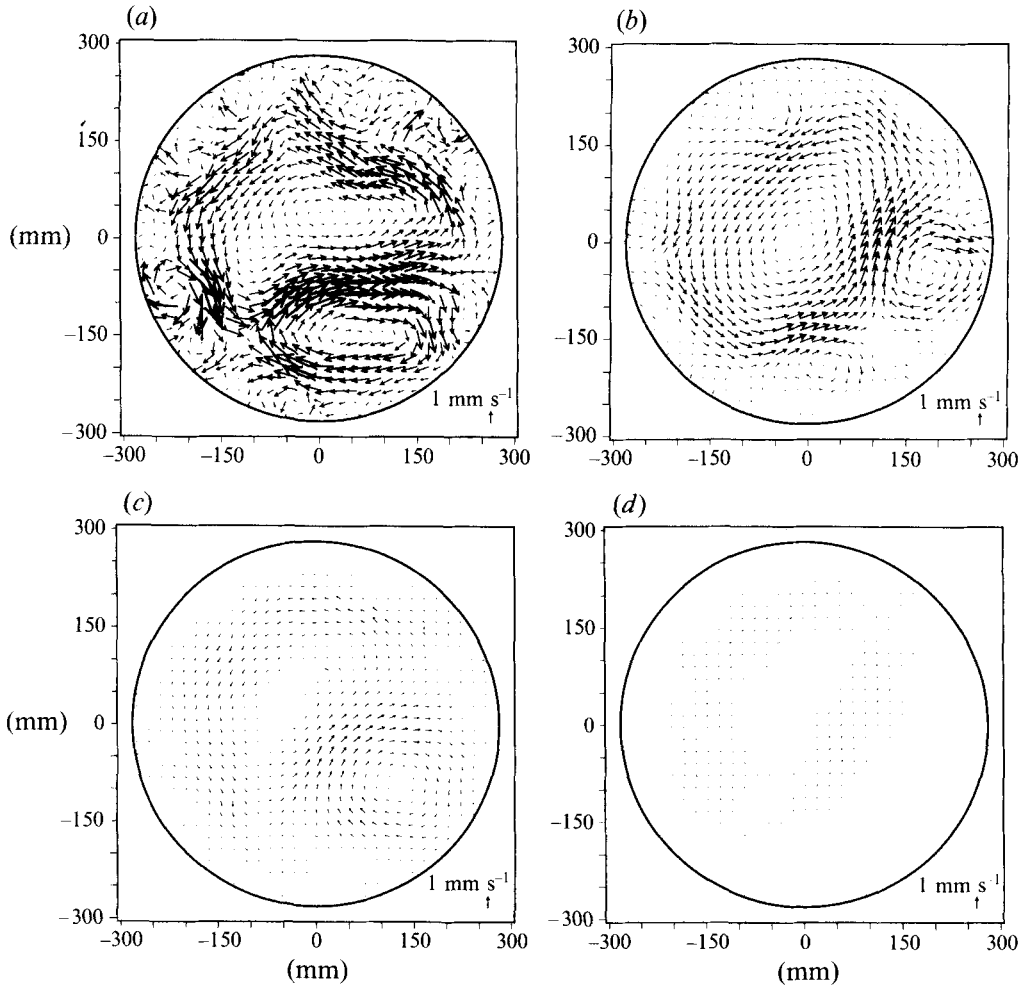
FIGURE 14. Stratified non-rotating flow forced by forty sources (Expt 6, $F = 0.48$, $Re = 1014$, $f/N = 0$). Velocity vectors are shown at the forcing level (*a*) and at height 20 mm (*b*), 50 mm (*c*) and 70 mm (*d*) above the forcing level. The flow was measured at $Nt = 900$ after the onset of forcing.

to become more geostrophic and, consequently, for it to be correlated over larger vertical scales. This property is shown in figures 14 and 15 for the non-rotating and rotating cases, respectively. Figure 14 shows velocity fields measured at the pumping level, figure 14(*a*), and at 20, 50 and 70 mm above the forcing level in figures 14(*b*), 14(*c*) and 14(*d*), respectively. These flows were measured by rapidly altering the vertical position of the light sheet. The measurements were taken 15 min after the forcing began and a large-scale circulation has been established and the flow remained steady on the timescale of the measurement period. The circulation is measurable at 20 and 50 mm above the forcing plane (figures 14*b* and 14*c*) but the motion is below the resolution of the plot at 70 mm (figure 14*d*). This structure is consistent with a viscous decay of the motion in the vertical, with a decay scale $2(\nu t)^{1/2}$ of approximately 60 mm.

The large-scale circulation penetrates furthest vertically and its vertical structure shows only slight changes in the shape of the vortex at different heights. The overall orientation and ellipticity of the circulation are constant with height. The small-scale eddies around the outer edge of the flow domain show a more limited vertical
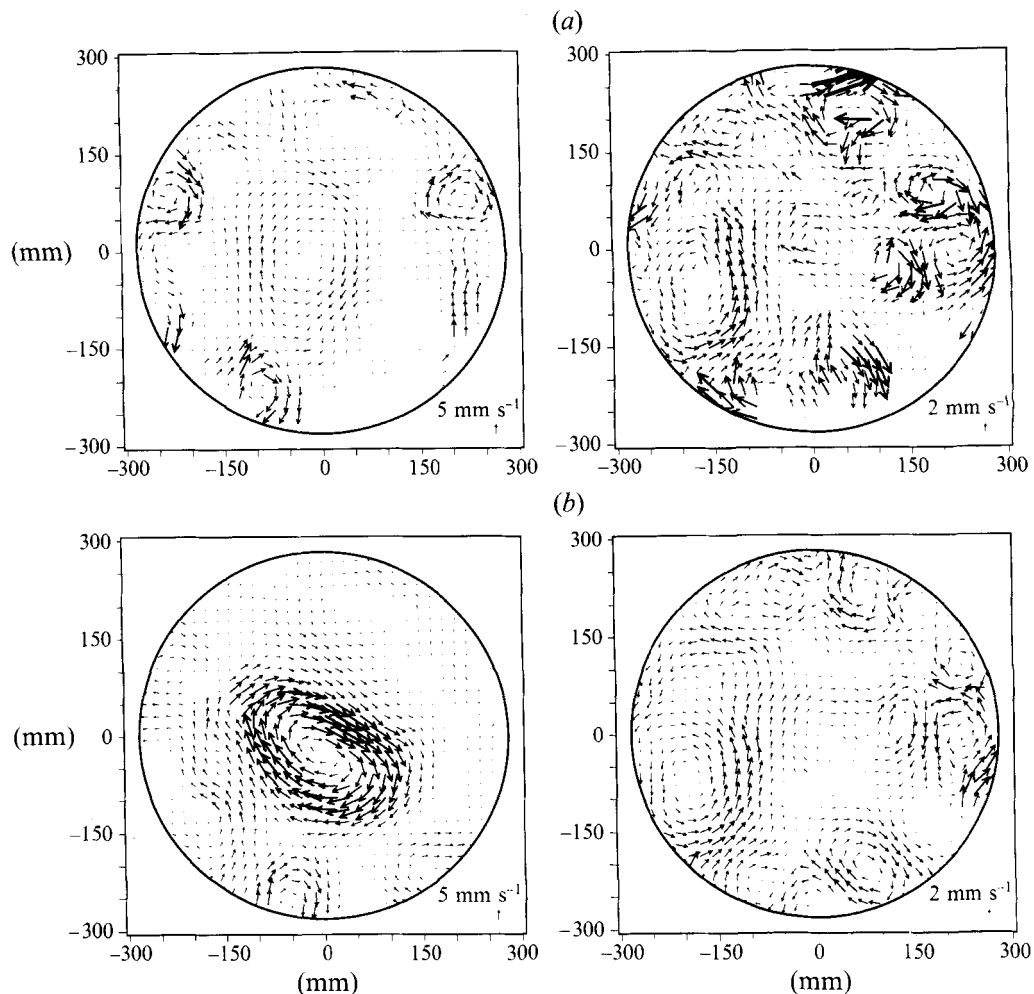
FIGURE 15. Stratified rotating flow observed at the forcing plane (left) and at the surface (right): (*a*) Expt 43, $F = 0.47$, $Re = 25600$, $f/N = 3.85$; (*b*) Expt 41, $F = 0.84$, $Re = 25600$, $f/N = 5.52$. The depth of fluid was 300 mm and the distance between the forcing level and the surface was 180 mm.

coherence. The large clockwise vortex at 5 o'clock is also visible at the 20 and 50 mm levels although its vertical axis is twisted. Typical values of the vertical shear of the horizontal velocity are 0.05 s^{-1} between the pumping level and a plane 20 mm above it, and above this the shears are weaker. This vertical shear will twist vertical vortex lines, and we can estimate the rate of reduction of vertical vorticity over the flow domain (area A) by $\omega\,(\partial v/\partial z)\,A^{-2}$. The rate of production of vertical vorticity by n sources is $(V^2/d)n$. Calculation of these quantities for Expt 6 shown in figure 14 gives values of 100 and 500 mm s^{-2}, respectively. Thus, to a first approximation, twisting of vortex lines is only a small fraction of the rate of production, consistent with the observation of the inverse cascade.

Two examples for rotating stratified flow showing the motion at the level of the forcing and at the surface are given in figure 15 for the cases $f/N = 3.85$ and 5.52. These measurements were taken at about 15 min after the beginning of forcing. We see that in these cases the motion has considerable coherence over a significant vertical separation (approximately 150 mm in both cases). Both flows show that the main

vortex structures extend throughout the depth of the flow, although some of the smaller-scale features do not. For example, in figure 15(*a*) at the surface we observe a large anticyclone in the centre, with three anticyclones and two cyclones around the outside of the domain. Each of these features can be clearly identified with a vortex at the forcing level. However, some of the smaller-scale features at the forcing level do not penetrate to the surface. For example, the anticyclone at 2 o'clock and the cyclone–anticyclone pair at 11 o'clock are not observed at the surface. It is interesting to note that the central eddy is more intense at the surface than at the forcing level (although the reason for this variation is not clear). For an eddy of radius R_E the vertical extent h is given by

$$h = BfR_E/N, \tag{1}$$

where the Burger number B is typically about 0.5 (Griffiths & Linden 1981). For these smaller-scale features $R_E \sim 50$ mm and so (1) implies $h \sim 95$ mm which is less than the distance (180 mm) from the forcing level to the surface. The anticyclone at 6 o'clock has $R_E \sim 70$ mm and (1) implies $h \sim 140$ mm, and this vortex is visible at the surface. The axes of the vortices are not exactly vertical and the large central anticyclone is twisted. The latter represents a vertical phase change which is consistent with extraction of baroclinic energy from the density field (see Griffiths & Linden 1981).

Similar properties are observed in the flow shown in figure 15(*b*). The larger-scale features are present throughout the depth of the fluid and, at this higher value of f/N, signatures of all the vortices present at the forcing level are observed at the surface. Again there are differences in shape of the vortices at the two levels, but their axes show more vertical alignment than those in figure 15(*a*). The smallest vortex, the cyclone at 10 o'clock has $R_E \sim 40$ mm and (1) implies $h \sim 120$ mm. Only a very weak signature of this vortex is visible at the surface, consistent with this estimate for the height scale.

These results show that, in the rotating case, the axes of the vortices are aligned approximately parallel to the rotation axis, and the horizontal and vertical scales correspond to a Burger number $B \sim 0.5$. This is equivalent to stating that the horizontal scale of the vortices is given by the Rossby deformation radius R_D corresponding to the *lowest vertical mode*. The vortices in figures 6–11 (and discussed in §4) show agreement between these two scales, and the observations presented in figure 15 show that the use of the full depth in calculating the Rossby deformation radius is appropriate.

6. Vorticity histograms

Further information on the development of the vortex structure in these flows can be obtained from an examination of the vorticity probability histograms. Figure 16 shows the probability histogram of the vorticity for Expt 6 which is a non-rotating flow with forty sources. The flow pattern for this experiment is shown in figure 4. Figure 16(*a*) shows the vorticity probability density distribution plotted over the development time of the flow. Each contour represents a measurement time during the evolution of the flow and the vorticity is plotted in dimensional units. At the initial time the flow is at rest and hence the distribution has a peak at the zero vorticity value. The zero vorticity line is indicated on each of these plots. As the flow evolves the vorticity spreads about the zero value as the fluid is accelerated from rest. We see, at later times, the development of a peak in the positive vorticity which corresponds to the anticlockwise large-scale circulation shown in figure 4(*d*). The negative vorticity is associated with flows around the edge produced by the sources. This variation over the
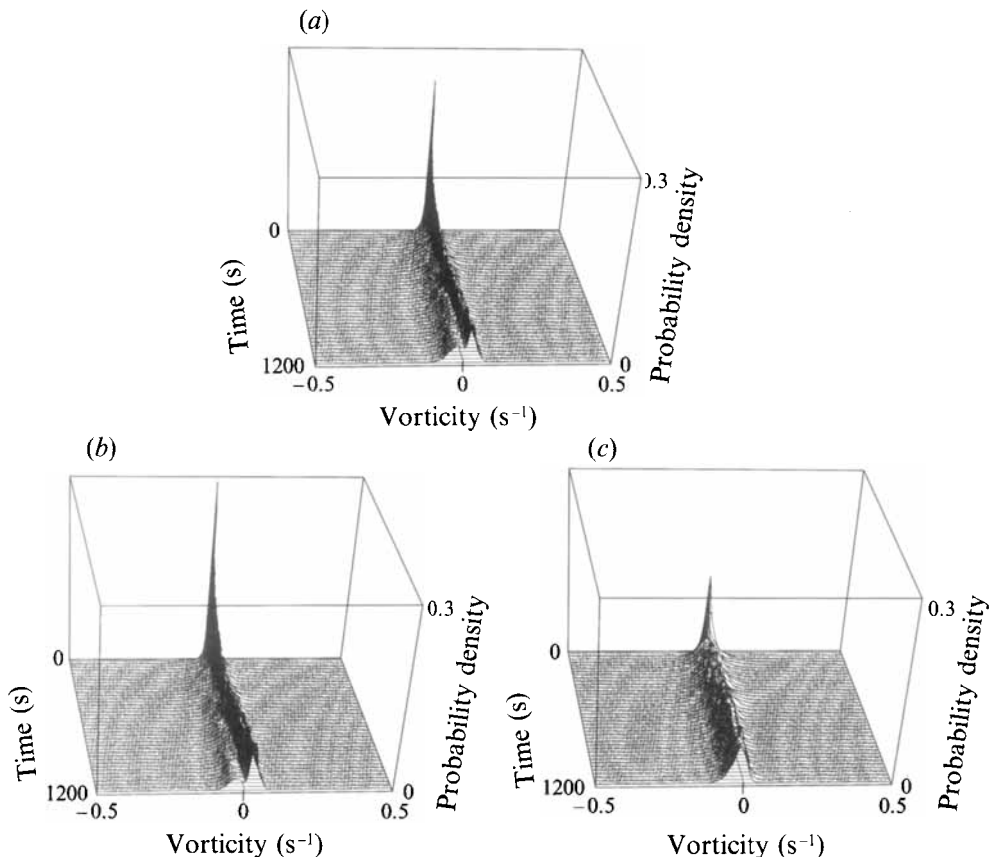
FIGURE 16. Vorticity probability density histogram for the non-rotating flow with forty sources. The flow here is Expt 6 shown in figure 4. The histogram for the whole flow domain is shown in (a) and the inner region (inside a dimensionless radius $r = 0.8$) in (b) and the outer region ($r > 0.8$) in (c). Vorticity maps are determined every 10 s from the velocity information and the histograms average the vorticity maps. The vorticity distributions are smoothed using a weak low-pass filter. The solid line shows the zero-vorticity contour.

flow domain is highlighted in figures 16(b) and 16(c) which show the histograms for the region inside a circle of dimensionless radius 0.8 in (b) and outside this circle in (c). (The circle shown in figure 4 corresponds to a radius of 1.) The inner region contains the large-scale circulation and this shows the high positive vorticity peak seen in figure 16(a). The outer region contains almost no flow with positive vorticity and the sources produce the negative-vorticity region as indicated in this figure. The extreme values of the positive and negative vorticity are very similar and the total average vorticity over the plane is very close to zero, as it must be from the constraint of zero circulation around the boundary.

The effect of varying the number of sources is shown in figure 17. These histograms correspond to the flows shown in figures 2, 3 and 4 for (a) eight sources, (b) twenty sources and (c) forty sources, respectively. In each case the qualitative behaviour is very similar with a peak appearing in the positive vorticity associated with the large-scale circulation. For the cases of eight and twenty sources shown in figures 17(a) and 17(b), respectively, there is a contribution to the negative vorticity associated with the outer edge of the large-scale circulation. For the forty-source case, figure 17(c), this
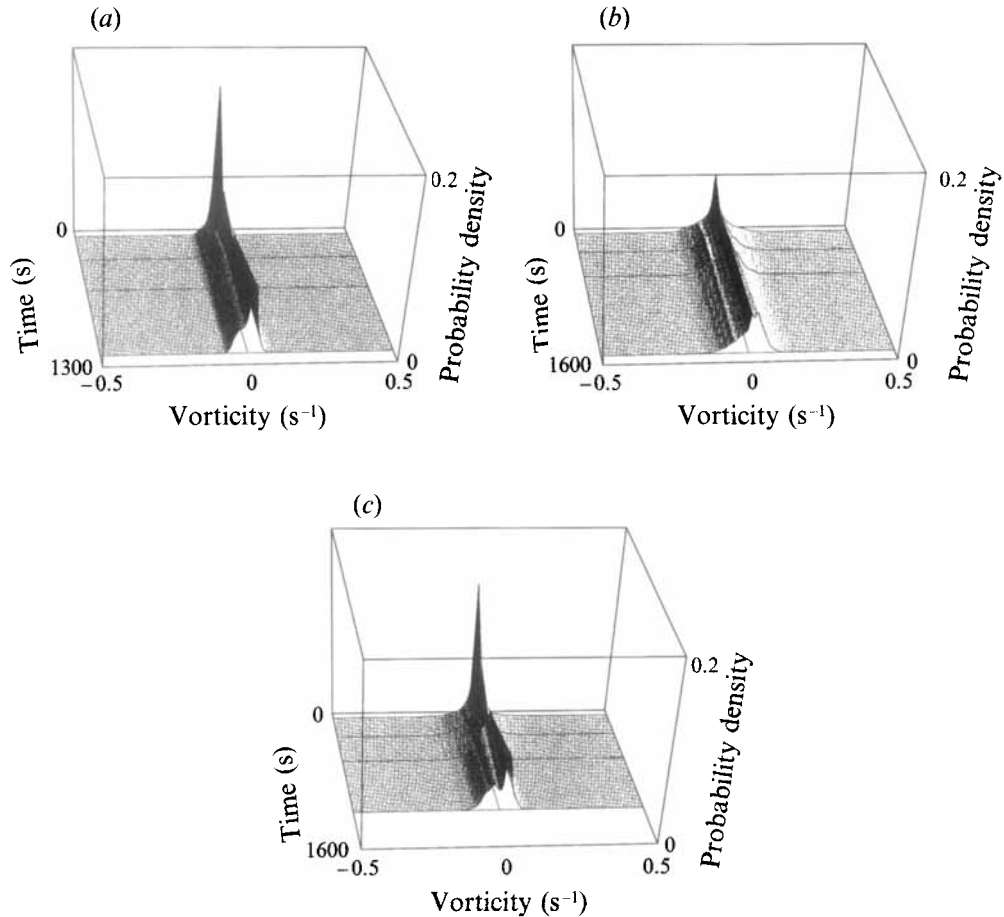
FIGURE 17. Vorticity histograms for non-rotating flows with (*a*) eight sources, (*b*) twenty sources and (*c*) forty sources. These correspond to flows shown in figures 2, 3 and 4, respectively. The vorticity was calculated at four times as shown on the figure and each represents a smoothed distribution.

distribution is more bimodal with the large-scale circulation containing positive vorticity almost exclusively. However, the evolution of these flows is qualitatively very similar for the range of source distributions studied and the values of the vorticity achieved in these flows is independent of the number of sources.

The effects of increasing rotation rate are shown in figure 18 which plots the distributions for increasing values of f/N: (*a*) $f/N = 0.8$, (*b*) $f/N = 1.6$ and (*c*) $f/N = 3.85$. The corresponding flows are shown in figures 6, 7 and 8, respectively. The effects of rotation change the qualitative appearance of these probability-density histograms. The spread in vorticity is increased and with increasing rotation rate the values of anticyclonic (negative) vorticity become considerably higher than those of the cyclonic vorticity. This asymmetry was observed in the structure of the flows (see figure 12) in which it was observed that the anticyclonic vorticity was clumped into isolated vortices while the cyclonic vorticity was smeared out throughout the flow. At the low rotation rate shown in figure 18(*a*) this asymmetry becomes apparent as the flow develops. In early times the flow produces two peaks in the vorticity associated with vortex pairs generated by the sources. As these flows evolve the cyclonic vorticity becomes slightly weaker and the anticyclonic vorticity is enhanced. The peak values of the Rossby
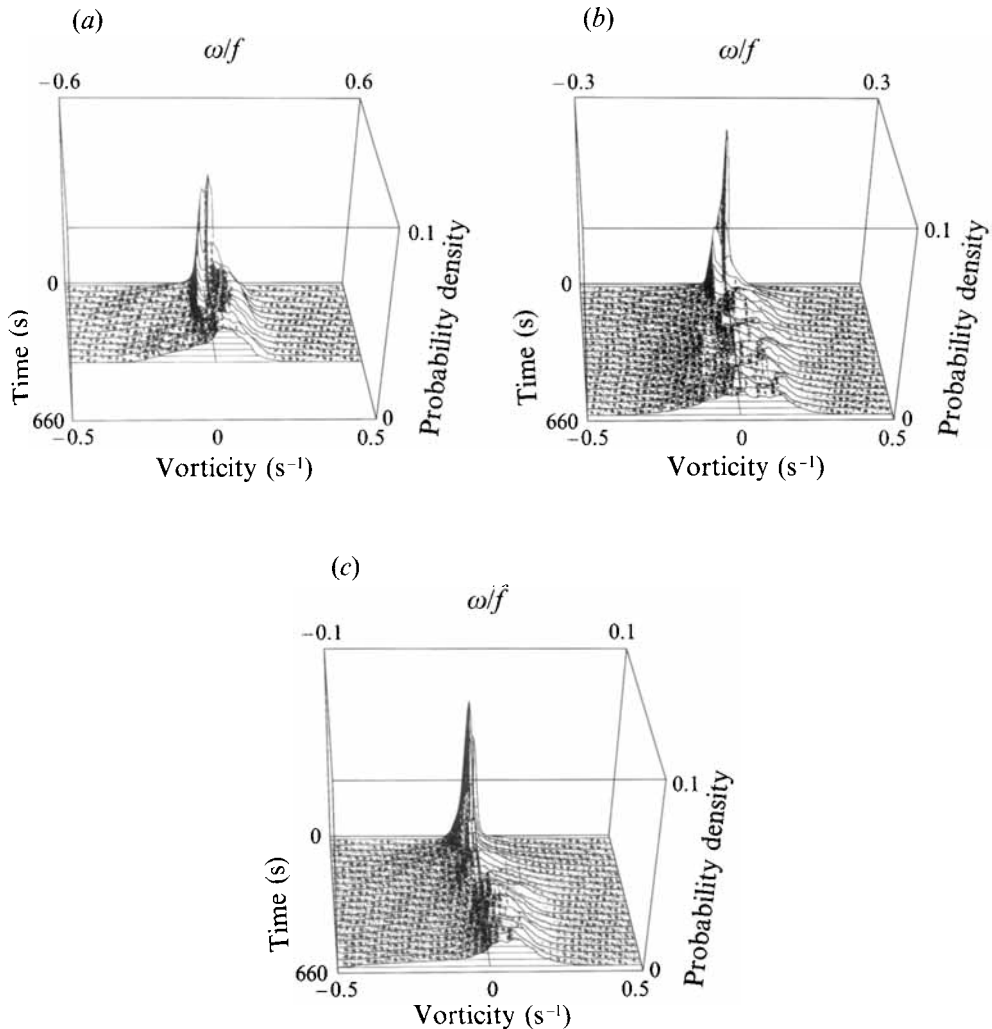
FIGURE 18. Vorticity histograms for the rotating flows shown in figure 12: (*a*) $f/N = 0.8$, (*b*) $f/N = 1.6$ and (*c*) $f/N = 4.0$. The vorticity axis shows both the vorticity in dimensional units and the Rossby number obtained by non-dimensionalizing the vorticity by the Coriolis parameter f.

number for the anticyclones corresponds to approximately 0.4. At the intermediate rotation rate shown in figure 18(*b*) there is an initial bimodal structure, again associated with the vortex pair formation at sources, but this rapidly breaks down into a wider distribution in vorticity. In the final state there is a wide range of vorticity values but again there is an asymmetry towards higher values in the anticyclones. The maximum Rossby number for these flows is again approximately 0.3. At the highest rotation rate studied, shown in figure 18(*c*), there is little evidence of a bimodal distribution in the vorticity field. The flow rapidly develops a broad range of vorticity and a clear asymmetry develops with intense anticyclones. The Rossby number of these anticyclones is approximately 0.15.

These vorticity histograms therefore quantify the behaviour observed and shown qualitatively in the earlier figures. We see clearly that at high rotation rates the anticyclonic vorticity is concentrated into isolated vortices while the cyclonic vorticity tends to be smeared out.

7. Discussion and conclusions

These experiments have investigated the response of a rotating stratified fluid to continuous forcing produced by a series of sources and sinks arranged symmetrically around the boundary of the fluid domain. The sources and sinks are located in a horizontal plane and so the flow is forced at a single (interior) level in the fluid. Since the sources are also directed horizontally and the stratification suppresses vertical motions when the forcing is weak enough, this method produces horizontal flow. Near the boundary the sources and sinks of spacing *l* produce horizontal eddies on a similar scale. These eddies propagate away from the boundary under the mutual interaction of their vorticity fields, further vortices are generated at the boundary and the whole flow domain fills with vortices.

To understand fully the role of the sources in forcing these flows, it is important to consider the origin of the asymmetry between the sources and sinks. To simplify our discussion we shall assume the sources and sinks to be two-dimensional. Similar arguments apply to the three-dimensional sources and sinks in this linearly stratified flow.

Kelvin's circulation theorem states that for an inviscid flow, the circulation around any closed contour (and hence, by Stokes' theorem, the vorticity contained within the contour) is constant. Thus, in the interior of the domain, the vorticity of a fluid element may only be changed through the action of viscosity. Near the boundary the forcing, however, has the ability to modify the vorticity in a more direct manner. Sinks remove fluid elements and the vorticity they contain, effectively breaking contours which were initially closed and so circumventing Kelvin's circulation theorem, while sources inject new vorticity.

A source has active control over the vorticity flux it creates. The vorticity is determined by a combination of the velocity profile across the orifice and the geometry of the orifice. Typically the vorticity will be confined to two strips, one containing positive and the other negative vorticity. The total vorticity contained in these two strips will be of equal magnitude so that the circulation around a contour enclosing all the flow from a given jet (i.e. both strips) will be zero. This balance is maintained even if the system is rotating.

In contrast a sink has only passive control over the vorticity flux through it. The vorticity associated with the fluid particles it withdraws is determined not by the sink, but by the entire flow. As a result we would expect small changes in the sink distribution (such as doubling the number of sinks and halving the mass flux through each) to have relatively little qualitative effect on the flow. In contrast, if the number of sources is doubled we would expect to see the type of changes which have been reported in this paper on increasing the number of source–sink pairs.

The forcing, then, may be considered as the injection of a pair of vortex strips and a corresponding mass flux at each source. Early in the development of the non-rotating flows the two vortex strips produced by each source will interact to form dipoles which propagate towards the interior. The dipole and the wake behind it carry the mass flux associated with the source. Subsequently, the motion induced by the vortex strip fragments already injected and modified by the combined effects of viscosity and advection by other vortex sheet fragments will lead to the more complex behaviour observed in the later stages of the development. This interaction is governed by the spacing of the vortex strips when they are at their strongest, principally when they are first injected before there has been time for viscosity to modify them. The diameter of the sources is important in that it sets the spacing between the dipole cores in the
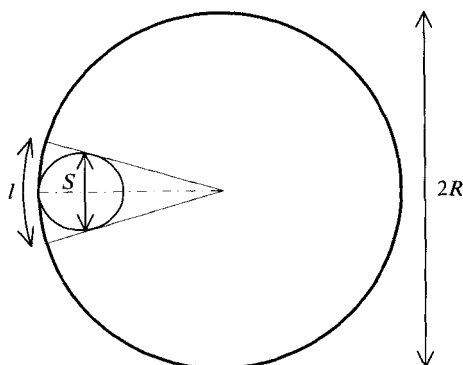
FIGURE 19. Diagram showing how effective spacing of the sources is defined.

absence of other interactions, while the spacing between the sources dictates how each of the possible dipoles interacts.

For a rotating system the relative vorticity of the vortex strips is again equal. If the sources introduced only vorticity we would expect a dipole to form and propagate in the same manner as seen in the early stages of the non-rotating flow. However, the flow associated with the sources is affected by the Coriolis force, which on the scale of the Rossby deformation radius turns the core of the jet issuing from the source to the right. As a result the negative (anticyclonic) vorticity strip gets turned back on itself to be concentrated into an anticyclone. At the same time the positive (cyclonic) vorticity gets stretched around the outside of this anticyclone to form a thinner, less-coherent, cyclonic strip. The injection of mixed fluid into a density gradient in a rotating fluid also produces a 'lens' which is a predominantly anticyclonic feature. This initial bias towards anticyclones may contribute to their ultimate dominance. However, it was observed that vortices of both signs were produced at low rotating rates, as can be seen, for example, in figures 18(a) and 18(b). At the higher rate of rotation in figure 18(c), anticyclones are formed preferentially from the start of the experiment.

The further time evolution depends on the relative strengths of the rotation (measured by the Coriolis parameter f) and the stratification (measured by the buoyancy frequency N). The controlling non-dimensional parameter is the rotational Froude number $Fr = f^2 R^2 / N^2 H^2$ where R is the radius and H the depth of the flow domain. This Froude number $Fr = (R/R_D)^2$, the square of the domain dimension to the Rossby deformation radius $R_D = NH/f$, for the lowest vertical mode of the system.

When $Fr \leqslant 1$, so that the Rossby deformation radius exceeds the domain scale, rotation is relatively unimportant and the flow evolves as though it were non-rotating. This case was discussed in §3, where the BDL experiments on non-rotating turbulence were extended by considering the effects of varying the forcing scale compared with the radius of the flow domain R. Similar results were found for all values of l/R in the range 0.16–0.80, in that an inverse energy cascade was observed. This upscale transfer of energy manifested itself as the development of a large-scale circulation in the interior of the domain which excluded the vortices produced by the forcing and kept them confined to the outer edge of the flow domain. BDL showed that vorticity was transported into the centre of the domain in order to maintain the large-scale circulation against dissipation. Similar diagnostics were not applied in the present experiments, but there is no reason to expect that the same processes do not apply.

Some variations in the structure of the flow were observed with changes in the forcing. The width of the streaming region in the large-scale circulation increases with

the number of sources and, since the energy of the flow also increases, the peak vorticity remains approximately constant. The eddies produced by the forcing have the same efflux velocities in the flows shown in figures 2, 3 and 4, and they are excluded from the interior of the circulation by a potential vorticity barrier of comparable strength in each flow.

In the non-rotating flows there are three lengthscales in the problem: L the size of the tank, R the radius of the ring and S the effective spacing between the sources. While the forcing is turned on, L appears to be of relatively little importance and we shall not consider it further here. The effective spacing of the sources is determined by how we may pack n structures of size S within the ring of radius R, where n is the number of source–sink pairs. Owing to the curvature of the ring, the effective spacing S will always be less than the perimeter spacing l. Figure 19 shows schematically the definition of S which may be evaluated from R and n as

$$S = \frac{2R\sin(\pi/n)}{1+\sin(\pi/n)}. \tag{2}$$

For convenience we define the dimensionless spacing

$$s = \frac{S}{R} = \frac{2\sin(\pi/n)}{1+\sin(\pi/n)} \tag{3}$$

to describe the ratio between these two lengthscales. For the present experiments we have $s = 0.55$ (eight sources), $s = 0.27$ (twenty sources) and $s = 0.15$ (forty sources).

The patterns shown in figures 2, 3 and 4 clearly show the dependence of the flow on the number of source–sink pairs. The size of the dominant eddies in the neighbourhood of the sources is approximately S, the effective spacing between the sources. Given the low Reynolds number of the jets forcing the flow, it is hardly surprising that the flow should adopt the scale of the forcing.

When there are only eight source–sink pairs (figure 2), $s = 0.55$ indicating that the size of the eddies is approximately half the radius of the tank. Thus the inner 50 % of the radius is available for regions of a different scale to develop. The inverse cascade of energy to larger scales causes this space to be filled by the largest structure possible, in this case an anticlockwise vortex. The cascade of enstrophy to smaller scales is also visible with the large velocity gradients on the edge of the eddies being formed through the interaction with neighbouring structures and, to a lesser degree, the interaction with the central circulation.

With the larger number of sources ($s = 0.27$, figure 4 and $s = 0.15$, figure 5) the size of the structures in the neighbourhood of the sources is much smaller. In this situation there is more space in the tank away from the perimeter for other scales to develop. Here we see again the inverse cascade of energy from the eddies around the edge into a single large structure in the centre of the tank. This structure is a robust feature of this flow and was found in all the experiments in this parameter regime.

As noted by BDL, these source–sink flows are not steady, but are turbulent and continue to evolve slowly on a timescale which is long compared with the eddy turnover time. In the perimeter eddies the turnover time may be estimated as S/V while it is $(R-S)/V$ for the central circulation. During the experiments we observed a steady global structure lasting many hours, while precise details of the interactions evolved in tens of seconds, the turnover timescale. Nevertheless, it was clear that the coherent structures generated by the sources were unable to penetrate the large-scale circulation. A similar partial barrier to turbulence is observed in the stratospheric ozone hole.

The effects of rotation are to inhibit this inverse energy cascade by causing baroclinic instability at the Rossby deformation scale R_D. The flow then evolves into a set of vortex structures with scales comparable with R_D. The vertical scale used to determine the deformation scale is the full depth of the flow, and the scales of the vortices are consistent with instability of the lowest vertical mode in the tank. In spectral terms energy is input at the scale of the separation of the sources. In the rotating flows this scale is fixed at 227 mm. For the lowest rotation rate ($f/N = 0.38$), shown in figure 6, $R_D = 750$ mm and so the energy presumably cascades upscale from the input wavenumber towards the deformation scale. In this case R_D is greater than the tank dimension and a domain-filling circulation develops. For the flows at higher rotation rates shown in figure 7 ($R_D = 190$ mm), figure 8 ($R_D = 92$ mm), figure 9 ($R_D = 75$ mm) and figure 10 ($R_D = 40$ mm) the energy input scale is greater than the deformation scale. Hence energy could cascade upscale to low wavenumber but all the scales would be above the deformation scale in these cases. At these high rotation rates the vortices forced directly by the sources are unstable to baroclinic instability and, with the exception of the flow in figure 7, we observe that the flow rapidly produces vortices at the deformation scale. In the flow shown in figure 7, the forcing scale and the deformation scale are comparable, and the initial flow develops in a manner very similar to the non-rotating case. Subsequently, the flow breaks down into a field of vortices with scales comparable to, but larger than, the forcing scale. This difference in behaviour is also observed in the vorticity histograms shown in figure 18. At the lowest rotation rate the vorticity is initially bimodal, reflecting the persistence of the forcing scale. At higher rotation rates, the breakdown to a flatter distribution occurs more rapidly.

The energy transfers in these rapidly rotating flows is not then simply an inverse cascade to low wavenumbers, with blocking at the (larger) deformation scale. This scenario was suggested by Griffiths & Hopfinger (1984) to explain the evolution of baroclinic instability of a large patch of buoyant fluid bounded by a front. In that case also the energy input scale is close to the deformation scale, and some growth in scale of the initial instability was observed. In the present experiments energy transfers to high wavenumbers by baroclinic instability. We do not envisage this process as a cascade, but rather a direct transfer over a wide range in wavenumber space, and it seems inappropriate to describe it as a local energy transfer. Transfers of energy both upscale and downscale in the same wavenumber range have been observed in numerical calculations in forced two-dimensional turbulence by Maltrud & Vallis (1991). In our experiments inverse cascade is also observed simultaneously with the transfer to high wavenumber, and is manifested by merging of vortices of like sign. However, unlike the numerical calculations where the flow was forced on two scales, only one forcing scale is required to observe these effects. The second scale is the naturally occurring deformation scale.

The way in which rotation increases the vertical coupling is not entirely resolved by these experiments. In a non-rotating stably stratified fluid at low values of the forcing parameter F, the motion is primarily horizontal and, apart from viscous or internal wave coupling, occurs independently at different depths (Metais, Riley & Lesieur 1994). Energy transfers to large scales take place at each vertical level, with some additional small-scale energy introduced by shear instabilities between the vertically uncoupled horizontal motions. Rotation produces a coupling between these vertical levels on a vertical scale set by the Burger number $h \sim fR/N$. Thus, as energy cascades to large horizontal scales the increase in R leads to increased vertical scales h in accord with this relationship. Since the vertical scale is ultimately limited by the depth of the

fluid, energy accumulates at R_D, the deformation scale based on the total depth H. This is a barotropization process occurring through balanced motions in the vortices. Vertical alignment occurs by nonlinear advective processes analogous to vortex interactions on a given isopycnal but the exact mechanisms by which these vertical interactions occur are not entirely clear.

At high rotation rates an asymmetry develops in the flow with the formation of strong anticyclones. The cyclones are generally weaker and less coherent features than the anticyclones. This result can be compared with recent numerical calculations of turbulence in rotating stratified flows by Metais *et al.* (1994). They observe a dominance of cyclones at low stratification. These cyclones occur on scales smaller than the forcing scales and are reminiscent of those produced in unstratified flows by grid stirring (Hopfinger, Browand & Gagne 1982). In more stratified situations they find both cyclones and anticyclones but do not report any predominance of anticyclones. Their calculations also show increased vertical coherence in the flow when the rotation rate is increased.

The Rossby numbers Ro of these vortices are finite but small (< 0.3) and hence the motions are expected to be quasi-geostrophic. The small vertical shears which are observed are consistent with these dynamics. It is, therefore, somewhat surprising that there is such a marked difference between the cyclones and the anticyclones. Similar robustness of anticyclones has been found in numerical calculations by Yamagata (1982), who suggests that it is due to nonlinearities in the geopotential surfaces associated with the eddies. In stratified flow anticyclones cause the isopycnal surfaces to dome at the centre of the vortex, while cyclones cause the density surfaces to diverge at the edges of the eddy. This difference in structure appears to make the anticyclones more coherent and stable structures.

REFERENCES

BOUBNOV, B. M., DALZIEL, S. B. & LINDEN, P. F. 1994 Source–sink turbulence in a stratified fluid. *J. Fluid Mech.* **261**, 273–303 (referred to herein as BDL).

COLIN DE VERDIERE, A. 1980 Quasi-geostrophic turbulence in a rotating homogeneous fluid. *Geophys. Astrophys. Fluid Dyn.* **15**, 213–251.

DALZIEL, S. B. 1992 Decay of rotating turbulence: some particle tracking experiments. *J. Appl. Sci. Res.* **49**, 217–244.

DALZIEL, S. B. 1993 Rayleigh–Taylor instability: experiments with image analysis. *Dyn. Atmos. Oceans* **20**, 127–153.

DRITSCHEL, D. G. 1993 Vortex properties of two-dimensional turbulence. *Phys. Fluids* A **5**, 984–997.

GRIFFITHS, R. W. & HOPFINGER, E. J. 1984 The structure of mesoscale turbulence and horizontal spreading at ocean fronts. *Deep-Sea Res.* **31**, 245–269.

GRIFFITHS, R. W. & LINDEN, P. F. 1981 The stability of vortices in a rotating, stratified flow. *J. Fluid Mech.* **105**, 283–316.

GRIFFITHS, R. W. & LINDEN, P. F. 1985 Intermittent baroclinic instability and fluctuations in geophysical circulations. *Nature* **316**, 801–803.

HOLFORD, J. M. 1994 The evolution of a front. Ph.D. dissertation, University of Cambridge.

HOPFINGER, E. J., BROWAND, F. K. & GAGNE, Y. 1982 Turbulence and waves in a rotating tank. *J. Fluid Mech.* **125**, 505–534.

LEGRAS, B., SANTANGELO, P. & BENZI, R. 1988 High resolution numerical experiments for forced two-dimensional turbulence. *Europhys. Lett.* **5**, 37–42.

McWILLIAMS, J. C.   1984 The emergence of isolated coherent vortices in turbulent flow. *J. Fluid Mech.* **146**, 21–43.

MALTRUD, M. E. & VALLIS, G. K. 1991 Energy spectra and coherent structures in forced two-dimensional and beta-plane turbulence. *J. Fluid Mech.* **228**, 321–342.

METAIS, P., RILEY, J. J. & LESIEUR, M. 1994 Numerical simulations of stably-stratified rotating turbulence. In *Stably-Stratified Flows – Flow and Dispersion over Topography* (ed. I. P. Castro & N. J. Rockliff). IMA Conference Series. Oxford University Press.

YAMAGATA, T. 1982 On nonlinear planetary waves: a class of solutions missed by the traditional quasi-geostrophic approximation. *J. Ocean Soc. Japan* **38**, 236–244.